

# Geologic Map of the Niobe Planitia Region (I-2467), Venus.

Iván López<sup>1</sup> and Vicki L. Hansen<sup>2</sup>

<sup>1</sup>Universidad Rey Juan Carlos

<sup>2</sup>University of Minnesota-Duluth

November 24, 2022

## Abstract

We present a 1:10M scale map of the Niobe Map Area (NMA) of Venus (0N-57N/60E-80E). Geologic mapping employed NASA Magellan synthetic aperture radar and altimetry data. The NMA geologic map, and its companion Aphrodite Map Area (AMA), cover ~25% of Venus' surface, providing with an important and unique perspective to study global and regional geologic processes. Both areas display a regional coherence of preserved geologic patterns that record three sequential geologic eras: the ancient era, the Artemis superstructure era, and the youngest fracture zone era. The NMA preserves a limited record of the fracture zone era, contrary to the AMA. However, the NMA host a diverse and rich assemblage of material and structures of the ancient era, and structures that define the Artemis superstructure era, with a footprint covering more than 25 percent of the surface of Venus. These two eras likely overlap in time and account for the formation of basement materials and lower plain units. Impact craters formed throughout the NMA recorded history. Approximately 40% of the impact craters show interior flood deposits, indicating that a significant number of NMA impact craters experienced notable geological events after impact crater formation. This and other geologic relations record a geohistory inconsistent with postulated global catastrophic resurfacing. Together, the NMA and the AMA record a rich geologic history of the surface of Venus that provide a framework to formulate new working hypotheses of Venus evolution, and to plan future studies of the planet.

# Geologic Map of the Niobe Planitia Region (I-2467), Venus

I. López<sup>1</sup>, and Vicki L. Hansen<sup>2</sup>

<sup>1</sup>Departamento de Biología y Geología, Física y Química Inorgánica. Universidad Rey Juan Carlos. 28933. Móstoles. Madrid, Spain

<sup>2</sup>Department of Earth and Environmental Sciences. University of Minnesota-Duluth. 1114 Kirby Drive, Duluth, MN 55812

Corresponding author: Iván López ([ivan.lopez@urjc.es](mailto:ivan.lopez@urjc.es))

## Key Points:

- We present a geologic map of the Niobe map area (0N-57N/60E-180E), representing about 13 percent of Venus' surface
- The map area displays an important imprint of the Artemis superstructure associated tectonic suites.
- Different volcanic styles locally resurface the map area, where different basement materials record the history of an ancient era.

## Abstract

We present a 1:10M scale geologic map of the Niobe Map area (NMA) of Venus (0N-57N/60E-80E). Geologic mapping employed NASA Magellan synthetic aperture radar and altimetry data. The NMA geologic map, and its companion Aphrodite Map Area (AMA), cover ~25% of Venus' surface, providing with an important and unique perspective to study global and regional geologic processes. Both areas display a regional coherence of preserved geologic patterns that record three sequential geologic eras: the ancient era, the Artemis superstructure era, and the youngest fracture zone era. The NMA preserves a limited record of the fracture zone era, contrary to the AMA. However, the NMA hosts a diverse and rich assemblage of material and structures of the ancient era, and structures that define the Artemis superstructure era, with a footprint covering more than 25 percent of the surface of Venus. These two eras likely overlap in time and account for the formation of basement materials and lower plain units. Impact craters formed throughout the NMA recorded history. Approximately 40% of the impact craters show interior flood deposits, indicating that a significant number of NMA impact craters experienced notable geological events after impact crater formation. This and other geologic relations record a geohistory inconsistent with postulated global catastrophic resurfacing. Together, the NMA and the AMA record a rich geologic history of the surface of Venus that provide a framework to formulate new working hypotheses of Venus evolution, and to plan future studies of the planet

## 1. Introduction

The NASA's Magellan mission collected a near-global synthetic aperture radar (SAR) data of the surface of Venus between 1990 and 1994, and revolutioning the knowledge of our sister terrestrial planet. One of the main results of this first global reconnaissance of Venus is that our neighbour planet lacks a system of moving plates like the one that operates here on Earth. However, an understanding of how Venus has evolved through time remains elusive. Paramount to unraveling the geodynamic evolution of a planet, Earth included, is to constrain the structures, materials and processes that have molded its surface, for which regional geologic mapping has proven to be a fundamental tool. Regional mapping provides a means to document and synthesize our current knowledge of a region or planet, and also serves as a tool to test working hypotheses, formulate questions, and devise new concepts to be studied in the future.

In this work we present a geologic map of the 1:10M Niobe Planitia Map Area (I-2467; 0N-57N/60E-180E). This map is part of a collaborative mapping project that includes the companion Aphrodite Map Area (AMA, I-2476), the object of a separate contribution [Hansen & López, 2020]. Together, both maps cover > 25% of Venus. The area includes different types of terrains, units, structures and volcanic styles representative of the surface of Venus. The map scale is well-suited for the discovery of regional to global scale processes, and to test current models of Venus geologic processes and evolution.

## 2. The Niobe Planitia Map Area (NMA)

The Niobe Planitia Region of Venus (I-2467) covers a surface of ~ 60,000,000 km<sup>2</sup> extending from lat 0° N to 57° N and from long 60° to 180° E (Figure 1). We refer to the map

area as the Niobe map area, or NMA, herein. NMA takes its name from Niobe Planitia, a large volcanic lowland province that occupies the central map area.

The NMA includes the northern part of western Aphrodite Terra, a topographically high region that extends  $\sim 10^\circ$  ( $\sim 1000$  km) on either side of the equator, including the crustal plateaus of western and central Ovda Regio and Thetis Regio, and several planitiae to the north. Tellus Regio, the third crustal plateau in the NMA dominates northwest NMA, defining the boundary between western planitiae. Elsewhere ridge belts (also called deformation belts) and/or large tessera-terrain inliers, forming locally higher regions, define the boundaries between planitiae in northern, central and eastern NMA.

Topographically the NMA ranges in altitude from over 5 km above mean planetary radius (MPR) in the equatorial highland regions to around 2.5 km below MPR in the lowlands of Leda and Atalanta Planitiae within northwestern and northeastern NMA, respectively. Llorona, Niobe, and Sologon planitiae, located north of the equatorial crustal plateaus, may form the northern part of a broad Artemis-concentric topographic trough [Hansen & López, 2020]. Akhtamar Planitia occupies southwestmost NMA whereas Rusalka Planitia occupies the southeast corner. Northern NMA includes from east to west: Atalanta, Vellamo, Tilli-Hanum, Lowana and Leda planitiae.

### 3. Data and Methods

#### 3.1. Image Data

Data for this study were provided by the U.S. Geological Survey (USGS) Astrogeology Team in the projection parameters (Mercator projection) for the Niobe Planitia Region (I-2467). The data are available online from the USGS Map-a-planet website (<https://astrocloud.wr.usgs.gov/>).

Cycle 1 (east-directed illumination, or left-looking) SAR images cover essentially the entire I-2467 map area, with local data gaps, particularly within central NMA. Cycle 2 (west-directed illumination, or right-looking) SAR data covers western NMA ( $60^\circ\text{E}$ – $120^\circ\text{E}$ ); cycle 3 left-look stereo SAR data is scarce and banded [Ford *et al.*, 1993]. Digital Compressed Once Mosaicked Image Data Records (C1-MIDR; 225 m/pixel) SAR data from the regional database and map base and digital full-resolution radar map (FMAP; 75–125 m/pixel) dataset were used in constructing the geologic map.

We also employed other ancillary non-SAR Magellan data available through the USGS Map-A-Planet website. The datasets include: (a) Topography (Global Topographic Data Record 3; GTDR 3); (b) Slope data (Global Slope Data Record; GSDR); (c) Reflectivity (Global Reflectivity Data Record; GRDR); and (d) Emissivity (Global Emissivity Data Record; GEDR).

GTDR data has an effective horizontal resolution of 10 km, and were combined with SAR images to produce synthetic stereo anaglyphs [Kirk *et al.*, 1992] using NIH-Image macros developed by D.A. Young. Synthetic stereo images played a critical role in elucidating the relations between geology and topography and, in particular, the interaction of flows, primary and secondary structures, and topography.

#### 3.2. Image Interpretation and geologic mapping

The interpretation of features in SAR images is key to developing a NMA geologic history. *Ford et al.* [1993] explored the subject of SAR image interpretation in depth. The methodology for defining geologic units and structural fabrics builds on standard geologic analysis detailed by *Wilhelms* [1990] and *Tanaka et al.* [1993], and employs cautions of *Hansen* [2000], *Zimbelman* [2001], *Skinner and Tanaka* [2003], and *McGill and Campbell* [2004]. Map units represent material emplaced within an increment of geologic history, to which standard stratigraphic methods have some limited application. Other units may be composite, in that the units might not be stratigraphically coherent over the entire represented area and (or) the material may have been emplaced over an extended period of time, particularly in relation to other units and (or) formation of secondary structures. In such cases the map units are descriptive units rather than temporal units. Attempts were made to clearly separate secondary structures from material units; location, orientation, and relative density of primary and secondary structures are shown independent of material units. Evidence for reactivation of secondary structures is common across the map area, which further complicates the process of unraveling both temporal constraints and geologic history. In addition, in many cases the designation of a material unit does not carry an implication of concurrent or synchronous emplacement [e.g., *Hansen*, 2000]. Indeed, absolute time is essentially impossible to constrain with regard to Venus geology at the time of this study.

Criteria for distinguishing discrete geologic units in the map area include (but are not limited to): (1) the presence of sharp, continuous contacts; (2) truncation of, or interaction with, underlying secondary structures and topography; and (3) primary structures, for example flow channels or edifice topography, that allow a reasonable geologic interpretation and which may also provide clues to three-dimensional geometry. Some mapped units do not fit these constraints, which limits their use in constructing stratigraphic interpretations. Composite units, in particular, do not provide reasonable temporal constraints, even of a relative nature. Composite character of the units is noted in the description of map units.

Estimating absolute geologic age is not currently possible for the surface of Venus. Unlike surface crater statistics for planetary bodies that have old surfaces and high crater densities, such as the Moon and Mars, Venus impact crater statistics cannot place constraints on the age of surface units that cover the small areas visible in the map area given the low density of craters and lack of small craters [*McKinnon et al.*, 1997; *Hauck et al.*, 1998; *Campbell*, 1999]. Relative age constraints may be established only where units are in mutual contact and (or) interact with the same suite of secondary structures. Such relative temporal constraints are only locally applicable and cannot be extended across the map area with confidence, nor are they valid for composite (time-transgressive) geologic units.

Geologic maps at all scales should provide the basis for interpreting geologic histories, which in turn provide critical relations for understanding the range of processes that contributed to the evolution of planets. Construction of a geologic map is a critical first step in unraveling geologic history. Geologic maps are interpretive products used in turn for further interpretation of geological processes [*Butler & Bell*, 1988; *Maltman*, 1990]. Therefore, mapping must be conducted in a fashion that ensures that any operative process can be discovered—that is, the mapping method must not predetermine the resulting geologic map [*Hansen*, 2000]. It is imperative, for example, that secondary structures (strain) be distinguished from geologic units because materials and structures record different ‘time slices’ in the evolution of Venus’ surface, and each reflect different aspects of the operative processes which formed overall geology [*Wilhelms*, 1972, 1990; *Hansen*, 2000; *North American Stratigraphic Code*, 2005]. In the

construction of this map we attempt to adhere to historical and contemporary terrestrial mapping methods, with particular attention to complementary criteria, format and cautions outlined for Venus [e.g., *Gilbert*, 1886; *Wilhelms*, 1972, 1990; *Compton*, 1985; *Butler & Bell*, 1988; *Maltman*, 1990; *Tanaka et al.*, 1993, 2010; *Hansen*, 2000; *Skinner & Tanaka*, 2003; *Zimbelman*, 2001; *McGill & Campbell*, 2004; *Grindrod & Guest*, 2006; *Hansen & López*, 2018].

In this contribution we identify and map: (a) geomorphic features and named features within the map area; (b) primary and secondary structures, most commonly lineaments formed during unit emplacement, or after unit emplacement, respectively; (c) material units; (d) non-material units such as ribbon-tessera terrain or shield terrain [e.g., lithodemic units; *North American Stratigraphic Code*, 2005]; (e) shock features or thin deposits that overlay material units or terrains (e.g., impact crater haloes, mantling material), shown as transparent stippled areas.

## 4. The NMA Geologic Map

This section describes the NMA geologic map (Plate 1). The NMA is composed of an assemblage of materials and structures that together record a spatially and temporally varied geohistory: (a) local basal terrains (crustal plateaus, lowland tessera inliers and other local basal units); (b) a suite of geological elements—tectonic and magmatic—associated with the formation of the Artemis superstructure [*Hansen & Olive*, 2010]; (c) regionally extensive suites of tectonic structures exposed across the lowlands, and local tectonic suites associated with individual tectonomagmatic features; (d) volcanic materials including: basal-shield transitional terrain and shield terrain [*Aubele*, 1996; *Hansen*, 2005], local volcano- and corona-related flow materials, and undivided volcanic materials; and (e) 146 impact craters.

### 4.1. Primary Structures, Secondary Structures, and Tectonic Fabrics

Different structures, both primary (depositional or emplacement-related) and secondary (tectonic), are identified in NASA Magellan SAR data. Tectonic fabrics represent suites of structures that together define a coherent structural pattern or fabric, and that may be genetically related.

#### 4.1.1. Primary structures

Primary structures are mostly related to volcanic and impact processes and include features such as channels, shields, pits/pit chains, lobate flow fronts and flow levees, and crater rims and impact-related haloes and splotches [*Ford et al.*, 1993].

Channels or canali are sinuous, low-backscatter troughs tens to thousands of kilometers long and a few kilometers wide; locally, they may lack apparent topographic relief; they are similar to terrestrial fluvial channels, interpreted to form by channelized fluid flow [*Baker et al.*, 1992, 1997; *Komatsu & Baker*, 1994]. A large section of Baltis Vallis, the longest channel on Venus (~6800 km), transects Atalanta Planitia in eastern NMA. Both the nature of the fluid and formational mechanism (constructive or erosional) are unknown [e.g., *Gregg & Greeley*, 1993; *Bussey et al.*, 1995; *Williams-Jones et al.*, 1998; *Jones & Pickering*, 2003; *Lang & Hansen*, 2006; *Waltham et al.*, 2008]. Canali could be primary constructional structures, related to levee

development during flow emplacement, secondary erosional structures that cut earlier emplaced material, or a combination of both.

Shields, interpreted as small volcanic edifices, are small (generally 1 to 15 km in diameter, rarely 20 km in diameter), quasi-circular to circular, radar-dark or radar-bright features with or without topographic expression and with or without a central pit [Guest *et al.*, 1992; Crumpler *et al.*, 1997; Addington, 2001]. The size of individual shields is difficult to constrain because bases of individual shields are typically poorly defined, and deposits commonly blend smoothly into a composite layer that cannot be treated as a time line or marker unit with any certainty [Hansen, 2005].

Intermediate volcanoes, such as steep-sided domes or tholi, represent volcanic features indicative of a relatively higher viscosity either due to a more felsic composition and/or differences in the texture or rate of the extruded magma [e.g., Stofan *et al.*, 2000; Pavri *et al.*, 1992].

Lobate flow fronts and flow levees developed within flow units can indicate surface flow direction, which in turn can provide information about flow emplacement and local topography at the time of flow emplacement.

Impact craters are perhaps most prominently marked by rims that sit above circular interiors and within/at the boundary of ejecta material marked by extremely radar-bright deposits [Weitz, 1993]. Some impact craters display haloes, radar-bright (rough) or radar-dark (smooth) deposits that extend outward from the rim and ejecta deposits up to many crater diameters [Izenberg *et al.*, 1994]. Haloes are thought to form as a result of the shock-induced crushing of host material just preceding or accompanying bolide impact or due to accumulation of fine-scale ejecta. Some craters have parabolic haloes that extend up to 20 crater radii to the west; these thin deposits(?) are interpreted as due to the interaction of east-to-west zonal winds [Whitten & Campbell, 2016; Campbell *et al.*, 2015; Campbell *et al.*, 1992; Arvidson *et al.*, 1991]. Numerous dark splotches also occur within the map area; these could represent bolides that exploded before impact [Kirk & Chadwick, 1994].

Crater haloes, parabolic deposits and dark splotches appear to degrade with time resulting in a decrease in radar contrast relative to surrounding terrain [Izenberg *et al.*, 1994]. Impact craters that display both extreme haloes and radar-bright crater interiors are generally interpreted as relatively young, whereas craters with degraded haloes, or lacking haloes entirely, and displaying radar-smooth filled interiors are interpreted as relatively old [Phillips & Izenberg, 1995; Herrick & Rumpf, 2011]. Impact crater haloes and dark splotches are indicated with a transparent map pattern so that underlying units and structures can be represented along with the extent of crater haloes.

#### 4.1.2. Secondary structures

Secondary structures or tectonic structures form after the emplacement of geologic units, and typically record tectonic processes. In addition, the distribution and (or) character of secondary structures may provide clues for the delineation of material units, as well as temporal relations between different material units [Hansen, 2000]. Secondary structures within NMA include various types of lineaments: (a) fractures and faults; and (b) broad ridges, folds, and wrinkle ridges. Given that the map area covers ~60,000,000 km<sup>2</sup> we cannot and do not show all lineaments. The focus here is an attempt to capture the essence of recognized structural suites. Therefore, in some cases lineament trends will be shown, in other cases each lineament is shown,

in yet other cases a collection of the lineaments is shown. There is no single unique scale of lineament or feature identification, just as there is no single unique scale of observation in the case of field-based mapping on Earth, particularly for maps that cover huge areas of Earth's surface.

Fractures are sharply defined lineaments with a negative, or null, topographic signature, commonly grouped into suites based on orientation, pattern (i.e., parallel or near parallel, radial or concentric) and/or spacing (that is, widely spaced or closely spaced). Fractures are generally interpreted as extensional structures [Banerdt *et al.*, 1997]. In some cases fractures appear as sets of paired lineaments, and may mark graben. Locally fractures consist of *en echelon* fractures indicative of either a shear fracture origin, or the emergence of a fracture at depth to the surface with the *en echelon* fractures marking hackles.

Some fractures in local radial suites transition to pits or pit chains, sharply defined depressions, or pit chains. Linear arrays of pits likely represent regions marked by subsurface excavation; they may mark the surface expression of dilatational faults or dikes [Grosfils & Head, 1994; Okubo & Martel, 1998; Bleamaster & Hansen, 2005; Ferrill *et al.*, 2004; Schultz *et al.*, 2004] or they could represent stopping features that would not require associated crustal extension [e.g., Cushing *et al.*, 2015]. Pits or pit chains can be considered primary structures or secondary structures, depending on the question at hand; pits are primary structures relative to pit-related materials, yet they may be secondary structures relative to the units they cut or are emplaced within.

Folds are ridges with a gradational radar character normal to their trend, and wave-like topographic expression; they are generally interpreted as contractional structures [Stofan *et al.*, 1993]. Small ridges are topographic ridges with low relief and width, similar in appearance to folds except that the nature of the lineaments is ambiguous—though possibly of contractional origin (marked by folds or thrust faults).

Wrinkle ridges define low sinuous structures spaced a few kilometers to tens of kilometers apart and up to a few hundred kilometers long. These lineaments, which represent low values of layer contractional strain (<2%), are found on most terrestrial worlds, especially on large flat expanses of volcanic flow materials [Watters, 1988; Banerdt *et al.*, 1997]. Locally wrinkle ridges occur as inversion structures formed by the inversion of fracture-fill material due to post burial contraction [DeShon *et al.*, 2000]. Wrinkle ridges typically form suites of near parallel structures (and occasionally orthogonal suites) formed over large regional expanses.

#### 4.1.3. Tectonic fabrics

Tectonic fabrics are an assemblage of related structural elements that together characterize a rock unit, as in the case of ribbon-tessera terrain [Hansen & Willis, 1996, 1998; Hansen, 2006].

Ribbon-tessera fabric is characterized by orthogonally developed suites of ribbons, or ribbon structures and folds. For a complete description of this tectonic fabric and its implications on the origin and evolution of tessera-terrain and crustal plateaus see Hansen & Willis [1996, 1998], Ghent & Hansen [1999], Brown & Grimm [1999], Hansen [2006] and Ruiz [2007]. For a discussion of ribbon-terrain controversies, see Gilmore *et al.* [1998], Hansen *et al.* [2000], and Hansen [2006].

Within the NMA we delineate ribbon-tessera ribbon and fold trends. Ribbon structures are shown as trends of ribbon ridges and troughs; fold structures demarcate fold crest or trough



trends. In most cases short-, intermediate, and long-wavelength folds define locally parallel trends [Hansen, 2006]. Graben complexes, common elements of ribbon-tessera terrain fabric, typically parallel ribbon trends. Graben complexes can be differentiated from ribbons on the basis of smaller length-to-width ratios—that is, graben complexes are generally wider and shorter than ribbon structures. Ribbon-tessera graben complexes typically cut at high angles to long-wavelength fold crests, commonly resulting in a lens-shape plan view. Some graben complexes define broad patterns (radial, concentric) that can could offer information on the evolution of the crustal plateaus after and during the formation of the ribbon-tessera fabric. Bindschadler et al. [1992] recognized ribbon, fold and graben structures within tessera terrain. These workers describe described ribbon structures as “narrow troughs”, clearly differentiating ribbon structures from generally parallel but morphologically different graben complexes.

## 4.2. Map Units

Map units interpreted across the NMA are broadly defined in this section. The map legend provides a complete description of units.

The contacts between adjacent units vary from well defined, whereas in other cases are approximate or gradational, due to the angular nature of individual contacts or the style of the units or terrains. For example, shield terrain (unit st), consists of a thin veil of numerous *in situ* locally sourced deposits associated with individual shields, typically on the order of a few km or less across [Guest et al., 1992; Hansen, 2005]; the location of the mapped contact could vary across 10s and locally perhaps even 100s of kilometers given the inherent challenges in recognizing individual shields and the wide variation in shield density [e.g., Hansen, 2005; Hansen, 2009; Hansen & Tharalson, 2014]. In the case of some basal terrains that were cut by fractures following basal unit formation and then later are locally buried by younger material, the contact between the basal terrain and younger units can be sharp, marked by fracture truncation. They can also be gradational, such as in cases in which the fractures are visible as lineaments, yet do not obviously cut the overlying material. In this case the overlying material is interpreted to form a thin layer across regions where earlier formed buried fractures are apparent as lineaments through the thin cover. The transition from a gradational to sharp contact can itself be very sharp or gradational. In addition, the amount/character of fracture burial can also be gradational.

### 4.2.1. Terrain Units

The term “terrain” describes a texturally defined region, for example, where tectonism imparted a surface with a penetrative deformation that disallows interpretation of the original unit or units [Wilhelms, 1990]. The characteristic texture of a terrain could imply a shared history, such as a terrestrial tectono-thermal history or an event that melds possibly previously unrelated rock units (any combination of igneous, metamorphic, and sedimentary rocks); no unique history is inferred or required prior to the event(s) that melded potentially separate units into the textural terrain (i.e., lithodemic unit). Events prior to terrain formation are unconstrained in time or process unless specifically noted. Three general classes of terrain units occur across NMA: ribbon-tessera terrain and associated units, basal terrain, and shield terrain and associated basal-shield transitional terrain.

#### 4.2.1.1. Ribbon-tessera terrain and associated units

Ribbon tessera terrain and associated intratessera basin units are widespread across the NMA marking the characteristic surface of crustal plateaus (Western Ovda/Manatun Tessera, and Ovda, Thetis, and Tellus regiones), and also occurring as lowland inliers. Units include the descriptive moniker plus the name of the host tessera region (e.g., Ovda or Tellus ribbon tessera terrain, rtO and rtT, respectively; or itbO and itbT). A descriptive term such as undivided (rtu) is applied to the relatively small exposures located in unnamed locations. Ribbon-tessera terrain exposures are typically characterized by orthogonal ribbon-fold tessera fabric [Hansen & Willis, 1998; Hansen, 2006]. Fold wavelengths range from less than one kilometer—essentially to the effective resolution of SAR data, to tens of kilometers. Ribbon wavelengths range from 2 to 5 km, and below, locally also to SAR effective resolution. Orthogonal ribbon-fold fabrics are the most common tessera fabric across NMA as they are for ribbon-tessera terrain globally [Hansen & López, 2010], but local shear fabrics [Hansen, 1992; Hansen & Willis, 1996] occur in central Ovda Regio and in tessera inliers in Niobe Planitia (e.g. Shimti-Kutue tesserae). Intratessera basin material, which typically fills short- to long-wavelength tessera-fold troughs (short-wavelength fold troughs are below the scale of the NMA), are best preserved and identified within crustal plateaus, although we delineate such units within large tesserae inliers. Tesserae inliers describe regional-scale linear to arcuate patterns in lowland basins. Given that inliers reside at low elevation and are locally embayed by younger volcanic materials, unique identification of intratessera basin material (as opposed to undivided volcanic material) can be difficult. For a more complete description of intra-tessera basin materials or the origin of crustal plateaus see Banks & Hansen [2000] and Hansen [2006].

#### 4.2.1.2. Local basal terrain

Local basal terrain is a term used to describe surfaces that lie within locally low stratigraphic positions relative to adjacent map units in planitiae. Similar to the naming scheme used in other terrain units we include the moniker basal terrain, and the name of the host planitia (e.g., Niobe or Leda basal terrain, btNi and btLe, respectively), or a descriptive term such as undivided (btu). These surfaces are termed terrains because it is unclear how many individual units might be represented, but the regions share suites or a suite of tectonic structures that formed prior to the emplacement of adjacent material. Local basal terrain exposures are just that, local, and there is no implication of shared histories between spatially separated basal terrain units across the NMA. However, it is also possible that isolated basal terrain exposures could locally represent temporal equivalent surfaces, or more likely perhaps, represent temporally equivalent unconformity bound packages (i.e., allostratigraphic surfaces/packages).

#### 4.2.1.3. Shield terrain

Shield terrain consists of thousands of individual shields and coalesced flow materials, referred to as “shield paint” for its apparent low viscosity during emplacement [Hansen, 2005; see also Aubele, 1996]. Shield paint could be formed from any combination of lava flows, air-fall deposits, or pyroclastic flows [Guest et al., 1992; Crumpler et al., 1997]. Shield terrain contains rocks with an interpreted shared emplacement mechanism (represented by primary structures),

which differs from ribbon-tessera terrain whose elements include an interpreted shared deformation history represented by secondary structures.

Within NMA, shield terrain material (unit st) is marked by distributed small (~1–10 km in diameter) shield edifices and their associated deposits. Unit st generally hosts a high density of shields although individual shield are not delineated within NMA due to the map scale. The contact of unit st with adjacent units can locally be sharp but is mostly gradational due to the point source nature of the volcanic activity. Unit st almost certainly represents a time-transgressive unit across the NMA [e.g., *Addington*, 2001; *Stofan et al.*, 2005], comprised of thousands of small edifices that may represent point-source, in situ, partial melting [*Hansen*, 2005]. This unit name is used in a descriptive fashion and does not imply temporal constraints.

We defined a unit transitional between shield and basal terrains, *basal-shield transitional terrain* (unit bst), wherein the discontinuous presence of shields and the low thickness of associated deposits reveal the tectonic structures of the underlying basal terrain. Similarly we locally observe other volcanic features (e.g., intermediate volcanoes and small coronae) partially embayed by shield terrain. Locally stratigraphic relations between such units and shield terrain are difficult to constrain due to the presence of shields in both units and to the point-source character of volcanism; we interpret a diachronic temporal relation between such units.

## **4.2.2. Material Units**

### **4.2.2.1. Volcanic material undivided**

Volcanic material undivided (unit vmu) represents a composite unit without stratigraphic significance that combines materials of different origin, and probably different age, that cannot be confidently differentiated with the available data. We use the unit name, volcanic material undivided, because the unit includes many different volcanic styles and radar textures, including corona-, volcano-, and shield-related material of low to intermediate-high backscatter and homogeneous to mottled texture. Volcanic and large tectonomagmatic features are distributed across unit vmu. Large flow units are difficult to delimit, perhaps due to the radar homogenization of the flows with time [*Arvidson et al.*, 1992]. Primary structures (e.g. channels, shields and flow fronts) provide evidence of the multiple genetic processes and distinct source locations for the materials that form the unit. Except for younger materials with clear contact relationships with these volcanic materials, most of the contacts of this unit are delineated as approximate or gradational when these units are in contact with basal-shield transitional and shield terrains; individual shields are also present in this unit. This unit correlates with unit flows undivided (unit fu) in the AMA [*Hansen & López*, 2020]. Both units are composite and lack stratigraphic significance across NMA and the AMA.

### **4.2.2.2. Volcano-related flows, fracture fed flows**

Several flow units in the NMA are variably associated with different types of volcanic structures (e.g., montes, tholi, paterae and fields of small volcanoes or colles) and can be differentiated from the undivided material. Each of these material units include the name of their associated volcanic feature (e.g., fmL, Lahar Mons flow material; fthE, Ezili Tholus flow material; fpM, Malintzin Patera; fsA, Aserat Colles shield fields and associated flows). The nature of the contacts vary for the different units; some units display clear flow margins that

allow delineation of contacts with sharp transitions; in other cases approximate contacts reflect situations in which the areal limit of the unit is not clear due to the nature and orientation of the radar contact and the interaction with secondary structures. Flow units associated with shield fields (e.g., units fsL, fsJ, etc.) display gradational contacts due to the point sourced nature of this type of volcanism. We differentiate these units from the shield terrain due to the larger size of the shields that form the volcanic field, the presence of associated flows and the local temporal relationship with unit vmu and other corona- and volcano-related units (i.e. locally postdate unit vmu). This differentiation between shield terrain and younger shield fields have been noted elsewhere on Venus [Addington, 2001].

#### **4.2.2.3. Corona-related material**

Many units within the NMA are corona-related deposits. The majority of the corona-related material units are spatially associated with individual coronae as indicated by the material unit name (e.g., fcI, Ituana Corona flows; fcE, Ereshkigal Corona flows), but in some cases where coronae are close or clustered, the unique origin of flows is unclear, and unit names indicate the names of the coronae or the region where these coronae are located (e.g. fcAt, Atalanta Planitia coronae flows). Some coronae have more than one unit delineated when it is possible to differentiate units at the map scale (e.g. Kunhild Coronae), but this is rare among coronae in the NMA. This could indicate different stages of corona evolution [e.g., Copp *et al.*, 1998, Smrekar & Stofan, 1999]. Nevertheless, absence of subunits does not mean that multistage corona evolution did not occur, but rather that we cannot identify multiple flows with existing data.

Contacts of corona-related material with locally older units bst and st are delineated as gradational given that individual shields are also present in the corona-related flows. The same applies to contacts between corona-related materials and shield fields and associated flow material.

#### **4.2.2.4. Crater material.**

The NMA includes two units that represent crater materials. Crater material undivided (unit cu) includes radar-bright material associated with impact crater formation, including crater ejecta and material inside the crater. Some craters present radar-dark interior deposits indicative of embayment by younger flows that cannot be represented at the scale of the map, although these deposits are visible in medium- and high-resolution images. The presence of such materials in individual craters is noted in the associated crater table (Table 1) but not differentiated in the map. This unit is descriptive with no implications for temporal equivalence across the map area. A second unit, crater associated flows undivided (unit cfu), represents impact melt or fluidized ejecta created by meteorite impact associated with the formation of individual impact craters; the melt could be impact related, fluidized ejecta, or formed as a result of tapping pre-existing subsurface magma. Exposures of this unit in most of the cases are small, and as such, not delineated as individual units associated with specific impact craters. Both units are descriptive, with no implications for temporal equivalence across the map area, these units are time-transgressive having formed in association with individual impact craters and not as lithostratigraphic packages.

### 4.3. Tectonic Structural Suites

Suites of tectonic structures define local or regional patterns that provide clues to operative tectonic or tectonomagmatic processes. We use the terms local and regional tectonic suites to delineate the different scale of tectonic suites. Local structural suites are generally spatially or geometrically associated with individual tectonomagmatic features such as coronae or montes. The timing of local structural suites likely corresponds to the formation, or stages of formation, of the individual features with which they are associated, although the development of these features and the related structural suites can be time-transgressive.

Regional structural suites describe coherent patterns across larger areas and commonly lack spatial or geometric correlation with individual geomorphic or geographic features. Temporal evolution of regional structural suites can be difficult to constrain given that these suites could form time-transgressively, and not necessarily formed at the same time across the expansive region where they are developed. Different surface units may be cut by a suite of regional structures, yet there is no guarantee that the entire suite of structures formed in a geological instance (or that there were not episodes of reactivation), frustrating efforts to interpret robust temporal constraints [Hansen, 2000].

#### 4.3.1. Regional Tectonic Suites

NMA's regional tectonic suites are best preserved within planitiae. Although planitiae are commonly considered featureless, NMA planitiae are characterized by numerous suites of distributed deformation features. The most obvious of these regional suites are contractional wrinkle ridges, low topography sinuous structures spaced a few kilometers apart and up to a few hundred kilometers long that record low (<2%) layer contractional strain. We define two groups or patterns of regional wrinkle ridges: (1) a broadly arcuate wrinkle ridge suite that extends from east to west across the NMA, broadly concentric to Artemis Chasma to the south [Hansen & Olive, 2010]; (2) a second regional wrinkle ridge suite, orthogonal to the first one, that fans from NW-trending in western NMA to NE-trending in eastern NMA; this suite is broadly radial to Artemis Chasma to the south. Four suites of distributed lineaments (interpreted broadly herein as fractures) also within the planitiae: (1) a fracture suite radial to Artemis Chasma to the south; (2) a suite of NW-trending lineaments that marks the western termination of Ganis Chasma to the east [Senske *et al.*, 1992]; (3) a suite of closely-spaced NE-trending lineaments; and (4) a suite of closely-spaced NW-trending lineaments. The perspective gained through the collaborative mapping of the AMA [Hansen & López, 2020] and the NMA allow us to assign the regional tectonic suites within the NMA to two groups: (a) suites related to the Artemis superstructure [Hansen & Olive, 2010]; and (b) other regional suites.

##### 4.3.1.1. Artemis superstructure-related suites

Structural suites related to the Artemis superstructure include extensive areal footprints: Artemis radial fractures (ARF; 12,000 km-diameter) and Artemis concentric wrinkle ridges (ACWR, 13,000-km diameter) [Hansen & López, 2018; Hansen & López, 2020; Hansen & Olive, 2010]. The first suite is broadly defined to include fractures, graben, dikes, lineaments, pit chains, stoping troughs, and describes a pattern radial to Artemis Chasma. This suite extends across most of NMA—well-preserved in central NMA and partly present in the west and

southeast. The suite is mostly absent in the northeast, as discussed in the geologic history. In Niobe, Sologon and Llorona planitiae several small coronae appear geographically related with ARF (e.g. Kubebe Corona in Llorona Planitia; Allatu, Bumiya and Dhisana coronae in Sologon-Niobe Planitiae). These features, referred to as circular-lows [Shankar, 2008], typically lack radial fractures.

The ACWR suite, previously described as circum-Aphrodite wrinkle ridges [Billoti & Suppe, 1999], defines a footprint concentric to Artemis Chasma [Hansen & Olive, 2010]. Wrinkle ridges are notably absent within ribbon-tessera and basal terrains, even in high-resolution SAR images; although wrinkle ridges locally cut intratessera basin material. Wrinkle ridges occur right up to the contact between ribbon-tessera terrain, basal terrain, and surrounding units, such as bst, st and vmu. These relations indicate that ribbon-tessera and basal terrain are not rheologically amenable to wrinkle ridge formation (that is, these units lack a thin deformable layer), whereas the thin basal-shield transitional terrain, shield-terrain, and unit vmu can form wrinkle ridge structures.

The ACWR suite cuts numerous flows associated with individual coronae or montes, providing clear evidence that such flows predated formation of this huge wrinkle-ridge suite. However, some corona-/mons-associated flows do not host wrinkle ridges; these relations could indicate that these flows formed after the Artemis-concentric wrinkle-ridge forming event, or that these flows were rheologically not amenable to wrinkle ridge formation, possibly due to flow thickness, internal flow structure, or composition. For example, most flows associated with Uti Hiata Mons (unit fmU1) do not show obvious development of wrinkle ridges, however, wrinkle ridges clearly cut the distal edges of these flows (unit fmU2). Thus, at least distal flows predated ACWR formation. If these flows post-dated formation of the ACWR suite, we might expect numerous examples illustrating the interaction of flows and pre-existing wrinkle ridge topography; however such relationships are not apparent. Some of the flows (e.g., proximal flows) might be too thick to have been affected by wrinkle ridge formation. It is also possible that Uti Hiata Mons formed during a period when some flows formed before and others formed after the Artemis - concentric wrinkle ridge- suite. The evolution and construction of a large volcano such as Uti Haita Mons, and the formation of a regional suite of wrinkle ridges are both likely to be time-transgressive, and plausibly each could last 10's to even 100's of millions of years.

The ARF and ACWR suites together define the Artemis superstructure, interpreted to have formed in association with the Artemis superplume [Hansen & Olive, 2010]. The ARF broadly pre-dates formation of the ACWR. At any one location concentric wrinkle ridges and radial fractures are mutually orthogonal. A second large suite of wrinkle ridges in NMA, orthogonal to ACWR, is interpreted to have formed due to inversion of buried ARF structures. Numerous Artemis-radial fractures locally 'end' abruptly where they are buried by younger deposits (e.g. volcanic material, undivided; corona-related flows); the fractures end, but transition into straight wrinkle ridges along trend. We interpret this occurrence of fractures and wrinkle ridges as early formed fractures that were buried and subsequently inverted during regional contraction to form topographically positive lineaments [e.g. DeShon et al., 2000]. Thus, we interpret the orthogonal pattern of wrinkle ridges in various planitiae to be the results of Artemis-concentric wrinkle ridges and orthogonal inversion structures.

#### 4.3.1.2. Other regional structural suites

We identify two regional fractures suites. These suites principally deform basal materials, but also occur locally in thin deposits that postdate basal units.

The NW-trending regional fracture suite extends across most of the NMA cutting units bst, st and vmu; it is dominately developed within bst in central and eastern NMA, and also occurs in Leda Planitia, northwest NMA. In Akhtamar Planitia (SW NMA), these fractures are locally restricted to basal materials in Lemkechen Dorsa and surrounding basal terrains. The fractures are closely spaced and relatively short, compared to ARF. Where these fractures cut basal materials and local volcanic materials adjacent to ribbon-tessera terrain, they parallel the trend of adjacent ribbon structures (e.g. locations around Gegute Tessera and Uni Dorsa in Niobe Planitia), consistent with structural reactivation of earlier-formed ribbon structure anistotropy.

NE-trending regional fractures mostly occur in Leda Planitia, and in isolated locations cutting units bst and st in Lowana and Llorona planitiae. Fractures in Leda Planitia are long and locally recognizable as paired lineaments, indicating that these are mostly likely graben; however, lineament orientation with respect to SAR acquisition is not optimal for characterization. Elsewhere these structures can only be resolved as lineaments, and display shorter lengths and closer spacing than in Leda Planitia. It is possible that these lineaments represent different genetic suites with similar orientation.

We suggest that the NW- and NE-trending suites predate ARF. Perhaps the most robust evidence for this relative timing emerges from broad geologic relations in which units vmu and st that locally bury the NW- and NE-trending fracture suites, are cut by ARF (e.g., 5°N-20°N/135°E-145°E).

#### 4.3.1.3. Fracture zones

The only fractures zone in the NMA is associated with the northwestern termination of Ganis Chasma, contrary to the AMA where fracture zones define an extensive tectonic domain [Hansen & López, 2020]. The part of Ganis Chasma expressed in the NMA lacks the topographic expression and fracture density that characterize the chasma closer to Atla Regio from which it radiates. Within the NMA spaced fractures and graben preserve the identity of host material they cut: ribbon-tessera terrain (Athena and Nemesis tesserae), basal terrain, and volcanic materials. Locally fractures covered by thin volcanic materials form inversion wrinkle ridges.

#### 4.3.2. Local Tectonic Suites

Local tectonic structures display linear, radial or concentric spatial patterns, typically associated with individual deformation belts, coronae or large volcanic features. We briefly describe areas of concentrated deformation, followed by suites associated with large tectonomagmatic features.

The NMA hosts several deformation belts (also called ridge belts) mark topographic boundaries between planitiae; parallelism of belt and internal structural trends that vary from belt to belt. Collectively the belts might be considered regional given their broad distribution across the NMA, but we consider them as local tectonic features herein: NW-tending Lemkechen and Unelanuhi dorsum in southwest NMA; NE-trending Mardezh-Ava Dorsa in central western NMA; N-trending Poludnista Dorsa in the southeastern most NMA; and the largest belts consisting of NNE-trending Vedma and Oya dorsum, and Nephele and Frigg dorsum, in Atalanta and Vellamo planitiae, respectively.

NW-trending Uni Dorsa and Lumo and Barballe dorsum differ from the deformation belts described herein. Uni Dorsa (800 km long) consists of ribbon-tessera with folds parallel to the dorsa (and ribbons normal to the dorsa); the tessera inlier is part of a larger quasi-circular ring of ribbon-tessera terrain together with Likho Tesserae, marking the boundary between Niobe Planitia and Vellamo Planitia. NW-trending Lumo and Barballe dorsum (500 and 1200 km long, respectively), spaced ~1000 km apart, comprise unit btu cut by NW-trending regional fractures.

NW-trending Lemkechen and Unelanuhi dorsum (200 and 2600 km long, respectively) form outcrops of discontinuous unit btu that predates local volcanic materials in Akhtamar Planitia. The outcrops are characterized by broad anastomosing dorsum-parallel ridges and folds. Wrinkle ridges that cut the young volcanic materials parallel the ridge belts and internal folds, but differ in morphology, size and spacing.

In northern Akhtamar Planitia, NE-trending Mardezh-Ava Dorsa (900 km long) includes NE-trending folds and fractures formed prior to the emplacement of material of the adjacent volcanic plains.

In southeasternmost NMA, and continuing to the AMA, Poludnista Dorsa (1500 km long) within Rusalka Planitia comprises a N-trending deformation belt that predated regional wrinkle ridges of the Artemis concentric suite (for a detailed structural analysis of Poludnista Dorsa see *Young & Hansen*, [2005]).

Large deformation belts in Vellamo and Atalanta planitiae describe a fan-shaped pattern with N-trending Nephele Dorsa (1900 km long) to the west and NNE-trending Vedma (3350 km long) and Oya (480 km long) dorsum in the east, and NNE-trending Frigg Dorsa in between. Nephele Dorsa forms a narrow belt of isolated exposures of btu; Frigg Dorsa is twice as wide but half the length. Vedma and Oya dorsum, which collectively extend from ~15° N to 55° N, are characterized by btu, cut by belt-parallel folds. Ribbon-tessera terrain occurs locally within Vedma Dorsa, although at a scale below map resolution. NW-trending lineaments within btu parallel local ribbon-tessera fabric trends. AWCRC in the surrounding units trend orthogonal to the deformation belt folds. Locally wrinkle ridges parallel the deformation belts and the expected trend of Artemis-radial fractures at such locations. These relations could be interpreted as reorientation of wrinkle ridges around still active deformation belts, or as reactivation of Artemis radial fractures. Both interpretations support a time-transgressive and non-singular history of wrinkle ridge formation in the NMA.

Local structural suites associated with individual coronae or volcanic features stand out prominently on the geological map. These suites are mostly radial and concentric fractures, with some isolated examples of volcanotectonic structures that show radial wrinkle ridges or concentric ridges. Individual radial or concentric suites formed during the evolution of their host feature, however there is no temporal equivalence inferred for spatially distinct radial or concentric suites.

Tectonomagmatic features that display local radial suites are grouped in four locations: (1) Akhtamar Planitia; (2) northern Lowana Planitia; (3) Atalanta Planitia; and (4) the equatorial highlands. Some radial fracture suites can extend great distances from their foci, and therefore might be useful as local temporal markers for unit delineation (i.e., Cinacoatl Mons in Atalanta Planitia and Kurukulla Mons in Till-Hanun Planitia).

In Akhtamar Planitia radial fracture suites connect large, otherwise isolated, tectonomagmatic centers (Hatshepsut Patera-H'uraru Corona, Uti Hiata Mons, Kaltash Corona, Kunhild Corona, Ereshkigal Corona), forming an extensive interconnected suite that might



appear similar to regional fracture zones. However, contrary to fracture zones in the AMA, these radial fractures do not obscure the identity of host materials. This tectonomagmatic chain extends southward into the AMA, connecting with an unnamed structured centered at 8° S/72° E and terminating in Ix Chel Chasma south of Ova Regio. This corona chain divides Manatum Tessera (western Ovda) from central Ovda Regio. Potential implications of this segmentation of the equatorial highlands remain to be studied.

In northern Lowana Planitia, radial fractures of Kurukulla Mons progressively change orientation to a N-S trend away from the magmatic center, parallel to the local ARF trend.

In Atalanta Planitia radial fractures with a focus of Cinacoatl Mons, extend >1000 km to the west with a ENE trend, likely the result of the operative regional stress field away from the volcanic source, at the time of fracture formation.

Similar to radial fractures associated with coronae in Akhtamar Planitia, other large local radial fracture suites occur in the equatorial highlands in the area that separates Thetis Regio and Haastte-baad/Gegute tesserae. Rosmerta and Blai coronae display radial fractures that extend 100's to 1000's of kilometers. Blai Corona connects with Ceres Corona to the southeast, part of the Diana-Dali corona-chasma chain in the AMA [Hansen & López, 2020]. The relationship of Rosmerta Corona with corona-chasma chains in the AMA is less clear. To the north, in the volcanic plains of Llorona planitia, radial fractures of Rosmerta and Blai coronae trend N.

Other local radial fracture suites associated with small features are typically areal restricted to the vicinity of their respective volcanic centers (e.g. Zaltu Mons and Heqet Corona).

Local concentric fractures are associated with many volcanic features (e.g. paterae-caldera and coronae). Most coronae in central NMA are ascribed to the calderic or circular lows subclass of coronae [e.g. DeLaughter & Jurdy, 1999; Shankar, 2008], characterized by concentric fractures similar to that of volcanic caldera, and lacking clear radial fracture suites.

Local folds suites that form concentric to some coronae (e.g. Ituana Corona), could be inversion structures (earlier-formed concentric fractures subsequently covered by thin volcanic flows), or gravity related structures [e.g. Sandwell et al., 1997].

A local suite of radial wrinkle ridges is restricted to Fedosova Patera; outward from the volcanic edifice the wrinkle ridges align with the adjacent ACRW. Different formation mechanisms for the formation of radial wrinkle ridges were discussed by Buczowski [2006] for the case of Irnini Mons.

#### 4.4. Impact Features

NMA hosts 146 impact craters, ranging from 1.9 to 98.1 km diameter. Table 1 lists impact crater location, diameter, elevation, crater density [e.g., Herrick et al., 1997], host material units, etc. Most of the craters are included in existing Venus crater data bases [e.g., Schaber et al., 1992; Herrick et al., 1997]. Each impact crater displays an interior, rim and ejecta deposit (unit cu); 40 percent have parabolic or halo deposits [e.g., Izenberg et al., 1994]. Central peaks are rare for craters with diameters <10 km. Impact crater deposits are shown as unit cu, crater material undivided, representing interior and ejecta deposits associated with local bolide impact. Each impact crater formed during a unique spatial and temporally localized event, therefore, composite unit cu is diachronous across the map area. Thus, unit cu is a descriptive unit, and does not imply temporal correlation. About 35-40% of the craters display interiors with radar-smooth material similar to the surrounding lowland material. Interior materials are too small to be represented at map scale but their presence is indicated in Table 1. These deposits are

interpreted as interior flood deposits that formed after, and unrelated to, initial impact crater formation [Izenberg *et al.*, 1994; Phillips & Izenberg, 1995; Herrick & Sharpton, 2000; Herrick & Rumpf, 2011]. Detailed mapping of Venus impact craters using high-resolution digital elevation models indicates that dark-floored craters with diameter >20 km have an average rim-floor depth of 290 meters and rim height (measured from rim to the adjacent surroundings) of 240 meters, less than bright-floored craters, indicating significant post-crater volcanic modification of radar-dark floored craters [Herrick & Sharpton, 2000; Herrick & Rumpf, 2011]. Thus, dark-floored craters likely predate, rather than post-date, the emplacement of at least some of the adjacent units (Hansen, [2000], figure 3 therein, for a possible mechanism). This means that the occurrence of an impact crater on a host unit cannot robustly indicate relative timing of unit and crater emplacement. Geologic mapping using high-resolution DEMs [e.g., Herrick & Rumpf, 2011] has not been employed in NMA construction.

Temporal relations between impact craters and tectonic events can be difficult to robustly constrain. If an impact crater lies between structural elements that comprise the local tectonic suite, such as wrinkle ridges or spaced fractures, the relative timing of crater formation and tectonic activity cannot be determined [Hansen, 2000]. Evidence for crater deformation (or lack thereof) is noted in Table 1 in cases where information can be extracted from map relations. At least nine craters show evidence of deformation, however, an apparent lack of deformation is not a robust positive test for impact crater formation after local tectonic activity given the spaced nature of tectonic deformation fabrics and the point location of individual craters. Of the craters that show deformation, six occur on ribbon-tessera and basal terrains, one on shield terrain and two on corona-related units.

Sixty craters locally cover Artemis-related structures. Twenty-two locally cover or follow Artemis radial fractures; forty locally cover Artemis concentric wrinkle ridges; two craters locally cover both. Although many of these craters have radar-rough (bright) interiors and halo deposits, consistent with relatively young ages [e.g., Izenberg *et al.*, 1994], at least twenty-seven of the craters that locally cover Artemis tectonic suites have interior fill that matches the radar reflectivity of their surroundings. These relations likely indicate a history of early Artemis-structure formation, followed by impact crater formation, following in turn by interior flooding of these individual craters.

Fifteen craters display crater-associated flow material, unit cfu. Ferrier and Cochram craters present flows are large enough to be mapped as individual units; however, these flows are included in unit cfu for mapping consistency. Ferrier and Himiko craters reside in regions marked by concentric fracture suites on the flanks of coronae. Both impact craters tapped into subsurface magma chambers, presumably associated with their respective coronae. Given the location of these impact craters on the flanks of coronae, and their associated outflow material, it is likely that their radar smooth interiors also relate to their locations relative to host coronae. The rest of the impact craters are not associated with magmatic centers; these features formed by impact on basal terrains and units bst and st. In these cases, the presumed sources of flows are subsurface magma chambers or magma accumulations near the surface but without manifestation in form of concentric fractures, or material produced due to the impact process (i.e. melting of the impacted materials).

These data and observations, independently and taken together with the observation that ~ 40% of the craters within the NMA show interior flooding, indicate that a significant number of impact craters within NMA experienced notable geological events (i.e., interior fill emplacement) after crater formation. These results are contrary to initial surveys of the Venus

crater population conducted using NASA Magellan data that concluded that only a few percent of Venus craters were deformed or embayed by volcanic material [Schaber *et al.*, 1992; Phillips *et al.*, 1992; Strom *et al.*, 1994; Collins *et al.*, 1999]. These new data are consistent with findings of Herrick and Rumpf [2011], and are difficult to accommodate within the context of catastrophic resurfacing models or any resurfacing models that require the vast majority of Venus impact craters to mark the top of the stratigraphic column [e.g., Turcotte, 1993; Strom *et al.*, 1994; Solomatov & Moresi, 1996; Turcotte *et al.*, 1999; Basilevsky & Head, 1998, 2000, 2002a, 2002b, 2006; Basilevsky *et al.*, 1997, 1999; Reese *et al.*, 2007; Romeo & Turcotte, 2010; Romeo, 2013; Ivanov & Head, 2015a,b; Kreslavsky *et al.*, 2015]. Thus, crater relations within the NMA cast doubt on the conclusions of these studies. In addition to the data described herein, a growing number of studies similarly indicate that hypotheses of catastrophic resurfacing, or hypotheses that call for late formation of most impact craters on Venus are inconsistent with geologic relations and/or modeling [e.g., Guest & Stofan, 1999; Herrick & Sharpton, 2000, 2002; Hansen & Young, 2007; Hansen & López, 2010; Hansen & Olive, 2010; Herrick & Rumpf, 2011; Bjonnes *et al.*, 2012; O'Rourke & Korenaga, 2015], and collectively challenge assumptions that the Venus crater population represents a limited, young, geologic time period.

## 5. Geologic History

A rich geologic history emerges from the geologic map of the NMA. Given the absence of elements of regional correlation we define local temporal relationships that help to constrain local geologic histories; however, these local histories cannot confidently be extrapolated across NMA or to Venus globally. Tessera terrain and other basal materials formed locally early, followed broadly by the time-transgressive evolution of the Artemis superstructure, coronae, montes, and lowland volcanic deposits.

Basal ribbon-tessera terrain units formed early across NMA and in a time-transgressive manner. That is, not all ribbon-tessera formed in one event, although these distinctive terrains likely formed within a geological era marked by specific geologic conditions, most notably an era marked by thin global lithosphere [Phillips & Hansen, 1994; Bindschadler, 1995; Hansen *et al.*, 2000; Hansen, 2006].

We distinguish three different groups of ribbon-tessera terrain: (a) within the equatorial crustal plateaus including west and central Ovda Regio and Thetis Regio, (b) within Tellus Regio, and (c) as inliers distributed across the NMA. All three groups of ribbon-tessera terrain present similar tectonic fabrics with local variations in trend and degree of embayment.

Ribbon-tessera tectonic fabric evolved through progressive deformation of a strong thin layer above an extremely low-viscosity layer over a strong substrate [Hansen, 2006], indicating a high heat flow across the areal extent of individual crustal plateaus [Ruiz, 2007], which are characterized by ribbon-tessera terrain. Tectonic fabric evolution was accompanied by formation of local intratessera volcanic basins filled with low-viscosity volcanic materials [Bindschadler *et al.*, 1992; Hansen & Willis, 1996, 1998; Gilmore *et al.*, 1998; Hansen *et al.*, 2000; Banks & Hansen, 2000; Hansen, 2006]. Evidence for this style of volcanic activity is preserved in Ovda, Thetis, and Tellus regiones due to high topography. However, clear differentiation between intratessera basin material and significantly younger volcanic material is difficult in tessera inliers due subdued topography (e.g. Haastse-baad Tessera).

Tectonic patterns in the ribbon-tessera inliers (e.g. Gegute and Haastse-baad tesserae in Llorona Planitia, Shimti, Kutue and Ananke tesserae crossing through Lowana, Niobe and Tilli-

Hanun planitiae; and Nemesis and Athena tesserae in Atalanta Planitia) show coherent patterns across regions similar in size to that of crustal plateaus [Hansen & López, 2010]. Such regionally coherent patterns across such expansive regions is consistent with the idea that ribbon-tessera inliers represent ancient packages similar to crustal plateau surfaces [Bindschadler, 1995; Ivanov & Head, 1996; Phillips & Hansen, 1998; Hansen & López, 2010].

Assemblages of basal terrain are exposed locally (e.g., unit btL), commonly in contact with ribbon-tessera terrain, and as isolated outcrops or kipukas. Origin of these basal terrains is not clear, nor is it required that all basal terrain formed in the same fashion. Basal terrains could have formed before, during, or after the era during which ribbon-tessera terrain formed, and could mark areas between regions of ribbon-tessera terrain. Exposures of basal terrain are cut by different tectonic structures. In some locations, these tectonic structures can be resolved only as close-spaced lineaments, but in most cases the tectonic structures appear to be comprised of closely-spaced fractures. In eastern NMA (e.g., Vedma Dorsa) NNE-trending outcrops of basal terrain are deformed by folds and broad ridges.

In central and western NMA regional NW-trending fractures cut basal terrain, with fractures parallel to adjacent tessera fabric trends; units bst, st and vmu postdate basal terrain. NW-trending fractures within younger volcanic units are due to incomplete burial, or structural reactivation, or both.

In northwest NMA NE-trending fractures cut basal terrain with fracture trends parallel to adjacent tessera fabric trend; NE-trending fractures both cut, and are covered by unit bst. Other local units (e.g., units st and fpHC) display NE-trending wrinkle ridges, parallel to, and in continuation of, fractures of the basal terrain; we interpret these wrinkle ridges as inversion structures of buried fractures [e.g. DeShon *et al.*, 2000]. All these previous materials and events would belong to the ancient era.

Various volcanic units, emplaced after tessera and basal terrain deformation, form the NMA volcanic plains. It is difficult to establish a singular chronology across the map area. Although the large tectonic suites of the Artemis superstructure (ARF and ACWR) constrain some temporal relations, evolution of the Artemis superstructure is not temporally constrained, and is likely time transgressive. Therefore, these suites cannot impose robust temporal constraints.

In the lowlands due north of Aphrodite Terra—the volcanic plains, composed mostly of units bst and st, also lack robust temporal relations. Unit st is composed exclusively by small shields, but local exposures of unit bst also present embayed intermediate volcanoes [e.g. López, 2011] and small coronae without evident associated flows (i.e. circular lows).

In general, ARF and ACWR cut units bst and st, although locally individual shields could postdate these tectonics structures. One possible mode of the formation of unit st (or bst) is heating from below by the Artemis superplume, driving *in situ* partial melting of the overlying crust and subsequent emergence of point-source shield formation. There is a possible spatial association, consistent with (but not requiring) a genetic association, between ribbon-tessera terrain and shield terrain. In western and central NMA, spatial association between units bst and st and ribbon-tessera terrain appears obvious, with large expanses of units bst and st located in and around large ribbon-tessera terrain blocks and inliers. In contrast, units bst and st are rare in Rusalka, Vellamo and Atalanta planitiae, all regions that generally lack ribbon-tessera terrain.

Large corona-related flow units that locally postdate units bst and st occupy a large region adjacent to Aphrodite Terra. These units (fcK, fcRo and fcOv) consist of low viscosity flows that extend great distances and postdate tessera, bst and st. Unit fcOv is a huge composite

unit composed of flows from several coronae and volcanic structures; this unit cannot be used as a detailed temporal marker. Some of material is easily traced to specific coronae, such as Kaltash (unit fcK), Rosmerta (fcRo) and Blai (fcB) coronae. These coronae, which formed on ribbon-tessera terrain, are characterized by large local radial fracture suites and topographically low corona annulus.

In this area it is also difficult to constrain temporal relations between coronae-related fractures and ARF structures. Flows of unit fcOv both cover and are deformed by ARF and ACWR; however, the composite nature of unit fcOv precludes the establishment of reliable temporal relations. Kaltash and Rosmerta coronae also display well-developed radial fracture suites, which further frustrate efforts to robustly constrain temporal relations with the Artemis-superstructure related suites. Given that ARF do not clearly transect these coronae, we expect that the coronae broadly post-date the formation of ARF; or rather, that the evolution of these coronae outlasted formation of ARF. However, ACWR cut distal flows sourced from Rosmerta Corona (e.g. unit fcRo). Thus it is possible that the Artemis superstructure began to form prior to the formation of Rosmerta, and formation of Rosmerta temporally overlapped with, and outlasted, that of the Artemis-superstructure.

In Akhtamar Planitia a cluster of tectonovolcanic structures postdate emplacement of local lowland materials. Temporal relations with regard to ARF and ACWR are difficult to constrain given that the local tectonic structures mimic the trends of these regional structures. The cluster formed by Ereshkigal and Kunhild coronae and their associated materials (units fcE, fcKu1 and fcKu2) has been interpreted as result of the formation of a now-extinct hot-spot [Herrick & McGovern, 2000]. Coronae-related materials are locally covered by younger volcanic flows associated with Ezili Tholus (unit fthE), a flat-topped volcano located northeast of the center of proposed extinct hot-spot (Ezili Tholus could be interpreted as part of late hot-spot evolution). Other large volcanic structures postdate the ARF and ACWR suites in Akhtamar Planitia. Uti Hiata Mons is a complex magmatic system with associated flow units (units fmU1 and fmU2) that locally postdate units bst, st and vmu and other previous volcanic structures (embayed intermediate volcanoes; see figures 4a and 4f in López, [2011]). Hatshepsut Patera (northern Akhtamar Planitia) represents a complex magmatic system composed of concentric fractures that define a caldera surrounded by flow material (unit fpH) and late steep-sided domes.

Collectively Kurukulla Mons, Hiei Chu Patera, Amra Tholus and several other unnamed volcanic structures comprise a large volcanic cluster located between northern Lowana Planitia and Tilli-hanun Planitia. Contact relations between materials associated with Kurukulla Mons and Hiei Chu patera (units fmK and fpHC) are difficult to constrain due to the absence of clear radar contacts and the presence of shields in both units; contacts are mapped as approximate. Flows from Amra Tholus and an unnamed volcanic edifice postdate radial fractures of Kurukulla Mons; however, it is not clear if these flows postdate all the activity in Kurukulla Mons or simply the formation of radial fractures. Temporal relations of all these units with respect to ARF and ACWR suites are difficult to determine given that radial fractures of Kurukulla Mons parallel ARF. ACWR cut some parts of units fmK, fpHC and fpul, however local wrinkle ridges suites, interpreted as inversion structures, also deform these materials.

In Lowana Planitia volcanic units associated with shield clusters or volcanic fields (units fsSh and fsLw) postdate units bst, st and vmu. The point-sourced nature of shields and the presence of shields in each unit renders contact delineation difficult; contacts are mapped as gradational.

Central NMA is dominated by units bst and st, which predate ARF and ACWR, and corona- and volcano-related units (fcA, fmUa and fpJ); the later units locally bury ARF but are cut by ACWR. In Niobe Planitia we interpret N-trending wrinkle ridges in unit vmu as having formed by structural inversion of ARF structures, with unit vmu locally postdating units bst and st, with Maa-ema Corona serving as a possible source for unit vmu.

In eastern NMA ribbon-tessera and basal terrain predate emplacement of composite units bst, st and vmu, and local corona- and volcano-related units (units fcI,fcV and unit fsL). In Rusalka Planitia corona-related flows locally postdate unit vmu (unit fu of *Young & Hansen*, [2003]). These corona-related materials (units fcRu1 and FcRu2) are in turn locally postdated by small volcano related flows (units fmI, fmLa and fmM) and volcanic materials associated with shield fields (units fsA, fsR and fsZy). The areal extent of unit vmu in the eastern NMA is more extensive than elsewhere; however, vmu is a composite unit with potentially many different sources. Unit vmu hosts numerous circular topographic rims that could represent buried coronae and that indeed could be source of at least part of this composite unit in this region. Eastern NMA also hosts a large number of volcanic channels or canali. Baltis Vallis, Venus' longest volcanic channel, runs through most of this part of the map area in unit vmu. Within Rusalka Planitia areally localized volcano-related units (fmZ) and materials related to shields fields (fsRk) postdate unit vmu. These shield-related volcanic materials are locally cut by Ganis Chasma fractures. Ganis Chasma is considered a young feature in the geologic evolution of Venus [*Basilevsky*, 1998]. Both the fracture density and topographic signature of the terminous of Ganis Chasma in the NMA are more muted than in Atla Regio, where recent volcanic activity has been proposed [*Shalygin et al.*, 2015].

In Atalanta Planitia a large corona-related composite unit formed by flows from different volcano-tectonic structures (Holde and Mari coronae, and Cinacoatl Mons) (unit fcAt) occupies much of northeastern NMA. This unit locally postdates basal materials and unit vmu; distal flows of unit fcAt postdate Baltis Vallis in Atalanta Planitia. These corona-related materials are locally covered by small shields and associated flows from Jurate Colles (unit fsJ), that also postdate unit vmu and tessera terrain of Ananke Tessera. Other local volcanic units sourced from fractures and volcanic centers postdate unit vmu in Atalanta Planitia (units fpF, fpU2 and ffr).

In western NMA the ACWR suite is well developed. NW-trending fractures could represent ARF, or fractures related to coronae and/or montes, or both; the trends fit both interpretations. Vellamo, Atalanta, and Rusalka planitiae display two suites of mutually orthogonal wrinkle ridges—ACWR, and parallel to ARF. It is likely that the latter suite represents buried ARF (by unit vmu) reactivated as inversion structures [e.g. *DeShon et al.*, 2002].

In general, the geologic history of the NMA is complex and diverse, with multitude of volcanic units that postdate basement materials. Most of these volcanic materials form composite units and we stress the importance that point-sourced volcanic activity played in the geologic evolution of the NMA (units bst and st), as first noted by *Aubele* [1996]. There also appears to be a broad spatial association of these units to ribbon-tessera inliers. Numerous coronae and large volcanoes form local clusters that postdate basement materials and basal plain materials (units bst and st). The main regional tectonic suites are related to the formation and evolution of the Artemis superstructure and can be used as a local relative temporal marker; however, one must be cognizant that the duration of Artemis superstructure evolution is unknown. Other regional and local tectonic suites deform the NMA materials and interact with volcanic flows depicting a rich and complex geologic history that can only be constrained locally in absence of reliable

temporal markers. Geologic relations preserved within the NMA do not support catastrophic resurfacing models, but instead are consistent with complex geologic evolution of the Venusian lowlands.

## 6. Conclusions

The geologic mapping of the NMA provide first-order observations and/or geologic implications enumerated below.

1. Geologic mapping of the NMA supports observations made in the AMA that show broad geologic domains, and broad cross-cutting temporal relationships in this part of the planet. Patterns are mostly defined by the mapping of structural elements that show coherent patterns across both map areas [Hansen & López, 2018]. The three tectonic domains defined in both map areas include, from oldest to youngest (Figure 2): 1) an Ancient era represented by ribbon-tessera terrain (including intra-tessera basin material) in both crustal plateaus and lowland inliers, and locally developed basal terrain; 2) Structures associated with the development of the Artemis superstructure, including Artemis-radial fractures and -concentric wrinkle ridge suites; and 3) a younger era characterized by the development of fracture zone terrain, including chains of coronae and chasmata.

2. The Ancient era is well represented by different lithodemic units distributed across the NMA (Figure 2). Ribbon-tessera terrain is found within the equatorial crustal plateaus (west and central Ovda Regio and Thetis Regio), Tellus Regio, and as inliers of different size scattered across the map area. Ribbon-tessera terrain units formed early across NMA and in a time-transgressive manner in an era marked by thin global lithosphere [Phillips & Hansen, 1994; Bindaschadler, 1995; Hansen et al., 2000; Hansen, 2006]. Other assemblages of basal terrain are locally exposed Basal terrains that could have formed before, during, or after the era during which ribbon-tessera terrain formed, and could mark areas between regions of ribbon-tessera terrain.

3. Shield terrain, a unique style of volcanic unit first recognized and described by Aubele [1996] in Niobe Planitia and later characterized in detail by Hansen [2005], occurs across much of NMA. Shield terrain postdates ribbon-tessera terrain inliers and basal terrains in lowland locations, however its evolution requires further study. This lithodemic unit likely formed broadly time-transgressive; it is not clear if formation of shield terrain started in the ancient era or later in the history of the volcanic plains, or both. Evidence for formation of shield terrain late within the ancient era, but perhaps relatively early within the Artemis superplume era includes: the occurrence of transitional materials between shield terrain and the basal units, and that shield terrain both cuts and is cut by Artemis Chasma-radial fractures; and yet Artemis Chasma-concentric wrinkle ridges (which post-date the ARF suite) generally cut shield terrain deposits. These relations lead most directly to temporal constraints in which shield within the NMA formed prior to and/or early during the evolution of the Artemis superstructure (that is, overlapping in time with the formation of the ARF suite), and was broadly emplaced prior to development of the extensive Artemis Chasma-concentric wrinkle-ridge suite—which represents late-stage evolution of this huge structure (Hansen & Olive, 2010). One would /could expect that the geologic transition between the ancient era and the Artemis superstructure era might be time-transgressive, rather than geologically catastrophic.

4. Artemis-radial fractures and Artemis-concentric wrinkle ridges defined regional patterns relative to Artemis Chasma (12,000 km and ~13,000 km diameters, respectively)

irrespective of the material units they deform (Figure 2), consistent with geologic relations documented within the AMA. Artemis radial fractures are more difficult to define in the NMA than in the AMA due to: the distance to Artemis Chasma; the location of the Aphrodite Terra crustal plateaus between Artemis Chasma and the NMA lowlands; and the occurrence of, and interaction with, other local tectonic suites. However, regional-scale map relations documents in both the AMA and the NMA together illustrate a clear pattern. Somewhat in contrast, the regional pattern of the Artemis-concentric wrinkle ridge suite is quite clearly defined within the NMA, particularly in southern and central NMA; equally important, this extensive wrinkle ridge suite is difficult to define in the north part of the NMA, which provides a boundary or spatial termination of this extensive suite. By comparison, the boundaries of this suite lie outside the spatial limit of the AMA.

5. Undivided volcanic materials and materials and local tectonic suites associated with individual tectonovolcanic structures postdate materials and structures of the ancient era. Much of this material likely formed during the era related to the evolution of the Artemis superstructure, or during the transition of this era to the youngest fracture zone era. It is difficult to establish a singular chronology across the map area. Although the large tectonic suites of the Artemis superstructure constrain some temporal relations, evolution of the Artemis superstructure is not temporally constrained, and likely time transgressive. Therefore, these suites cannot impose robust temporal constraints. Some tectonovolcanic structures seem to postdate, or at least have outlasted, formation of the Artemis superstructure given that associated flows are not apparently deformed by the Artemis-concentric wrinkle-ridge suite. However, such flows could also predate wrinkle-ridge formation, given that that individual flows, or parts of flows, could be rheologically unfavorable to the formation of wrinkle ridges. Geologic relations documented within NMA are consistent with a time-transgressive transition from the Artemis superstructure era to the fracture zone era.

6. The Fracture Zone Domain era is little represented in the NMA compared to the AMA. In the NMA we observe the termination of fracture zones (e.g. Ganis Chasma) where fracture density is lower than in the fracture zones observed in the AMA, and where precursor materials can be observed. Coronae within NMA, particularly those near the southern boundary with AMA (e.g., Blai, Rosmetra, Kaltash) could represent distal limits of the fracture zone domain, which includes coronae and chasmata. Further study, including more detailed geologic mapping may shed light on these relationships.

7. Impact craters clearly formed time-transgressively across the NMA relative to each of the three major geologic eras noted above, with near half of the craters within the NMA show interior flooding, indicating that a significant number of impact craters within NMA experienced notable geological events (i.e., interior fill emplacement) after impact crater formation. Thus, there is no geologic evidence within the NMA that impact craters lie at the highest level of NMA stratigraphy, and thus that impact craters formed as the youngest 'event' across the NMA. Furthermore, geologic relations do not require, and in fact provide strong evidence against, global-scale catastrophic resurfacing of Venus.

8. NMA materials and structures depict a rich and complex geologic history that can only be constrained locally in absence of reliable temporal markers. Geologic relations preserved within the NMA do not support catastrophic resurfacing models, but instead are consistent with complex geologic evolution of the Venusian lowlands.



In summary, the picture that emerges is the regional coherence of preserved geologic patterns in this part of the planet (both AMA and NMA), that record three relatively distinct geologic eras with the first two particularly well recorded within the NMA [Hansen & López, 2018]. The three eras are relatively distinct in terms of the geologic elements that define them. However, the temporal transition from one era to the next does not appear to be sharply defined, and as such may represent global-scale geodynamic transitions indicative perhaps of transitional geodynamic processes. Future geologic mapping of the rest of Venus, at a similar scale to that presented herein, will add important spatial and temporal information regarding the evolution of these three geologic eras and could also lead to the identification of other geologic eras within the evolution of Earth's sister planet Venus.

## Acknowledgments and Data

Geologic mapping was supported by National Aeronautics and Space Administration (award NNX12AQ71G). Base maps used for geologic mapping are available free in Zenodo (López and Hansen, 2020, <http://doi.org/10.5281/zenodo.3712688>). NASA Magellan data are available via USGS Map a Planet website (<https://astrogeology.usgs.gov/tools/map-a-planet-2>). V. L. H. gratefully acknowledges support from the McKnight Foundation and the University of Minnesota. The authors have no financial conflicts of interests or other conflicts of interest with regard to this work.

## References.

- Addington, E. A. (2001). A stratigraphic study of small volcano clusters on Venus. *Icarus*, 149, 16–36.
- Arvidson, R. E., Baker, V. R., Elachi, C., Saunders, R. S., Wood, J. A. (1991). Magellan: Initial analysis of Venus Surface modification. *Science*, 252, 270–275.
- Arvidson, R. E., Greeley, R., Malin, M. C., Saunders, R. S., Izenberg, N., Plaut, J. J., Stofan, E. R., Shepard, M. K. (1992). Surface modification of Venus as inferred from Magellan observation of plains. *Journal of Geophysical Research-Planets*. 97, 13303–13318.
- Aubele, J. (1996). Akkriva small shield plains; definition of a significant regional plains unit on Venus. *Lunar and Planetary Science Conference*. 27, 49–50.
- Baker, V. R., Komatsu, G., Parker, T. J., Gulick, V. C., Kargel, J. S., Lewis, J. S. (1992) Channels and valleys on Venus—Preliminary analysis of Magellan data. *Journal of Geophysical Research-Planets*. 97, 13395–13420.
- Baker, V. R., Komatsu, G., Gulick, V. C., and Parker, T. J. (1997). Channels and valleys, in Bouger, S.W., Hunten, D.M., and Phillips, R.J., eds., Venus II: Tucson, University of Arizona Press, 757–798.
- Banerdt, W. B., McGill, G. E., and Zuber, M. T. (1997). Plains tectonics on Venus, in Bouger, S.W., Hunten, D.M., and Phillips, R.J., eds., Venus II: University of Arizona Press, 901–930.
- Banks, B. K., and Hansen, V. L. (2000). Relative timing of crustal plateau magmatism and tectonism at Tellus Regio, Venus. *Journal of Geophysical Research-Planets*. 105, 17655–17668.
- Basilevsky, A. T. (1998). Age of rifting and associated volcanism in Atla Regio, Venus. *Geophysical Research Letters*. 20, 883–886.

- Basilevsky, A. T., and Head, J. W. (1998). The geologic history of Venus: A stratigraphic view. *Journal Geophysical Research-Planets*. 103, 8531–8544.
- Basilevsky, A. T., and Head, J. W. (2000). Geologic units on Venus: Evidence for their global correlation. *Planetary and Space Science*. 48, 75–111.
- Basilevsky, A. T., and Head, J. W., (2002a). On the rates and styles of late volcanism and rifting on Venus. *Journal Geophysical Research-Planets*. 107, no. E6, doi:10.1029/2000JE001471.
- Basilevsky, A. T., and Head, J. W. (2002b). Venus: Timing and rates of geologic activity. *Geology*, 30, 1015–1018.
- Basilevsky, A. T., and Head, J. W. (2006). Impact craters on regional plains on Venus: Age relations with wrinkle ridges and implications for the geological evolution of Venus. *Journal Geophysical Research-Planets*. 111, E03006, doi:10.1029/2005JE002473.
- Basilevsky, A. T., Head, J. W., Schaber, G. G., and Strom, R. G. (1997). The resurfacing history of Venus, in Bouger, S. W., Hunten, D. M., and Phillips, R. J., eds., *Venus II: Tucson*, University of Arizona Press, 1047–1086.
- Basilevsky, A. T., Head, J. W., Ivanov, M. A., and Kryuchkov, V. P. (1999). Impact craters on geologic units of northern Venus: Implications for the duration of the transition from tessera to regional plains. *Geophysical Research Letters*. 26, 2593–2596, doi:10.1029/1999GL008329.
- Billoti, F., and Suppe, J. (1999). The Global Distribution of Wrinkle Ridges on Venus. *Icarus*. 139, 137–157.
- Bindschadler, D. L. (1995). Magellan: A new view of Venus' geology and geophysics. *Reviews of Geophysics*. 33, 459–467.
- Bindschadler, D. L., deCharon, A., Beratan, K. K., and Head, J. W. (1992). Magellan observations of Alpha Regio—Implications for formation of complex ridged terrains on Venus. *Journal of Geophysical Research-Planets*. 97, 13563–13577.
- Bjonnes, E. E., Hansen, V. L., James, B., and Swenson, J. B. (2012). Equilibrium resurfacing of Venus: Results from new Monte Carlo modeling and implications for Venus surface histories. *Icarus*, 217, 451–461, doi:10.1016/j.icarus.2011.03.033.
- Bleamaster, L. F., III, and Hansen, V. L. (2005). Geologic map of the Ovda Regio quadrangle (V-35), Venus. *U.S. Geological Survey Scientific Investigations Map I-2802*, 1:5,000,000, <http://pubs.usgs.gov/imap/i2808/>
- Brown, C. D., and Grimm, R. E. (1999). Recent tectonic and lithospheric thermal evolution of Venus. *Icarus*, 139, 40–48.
- Bussey, D. B. J., Sorenson, S. A., and Guest, J. E. (1995). Factors influencing the capability of lava to erode its substrate: Application to Venus. *Journal of Geophysical Research*, 100, 16,941–16,948.
- Butler, B. C. M., and Bell, J. D. (1988). *Interpretation of Geological Maps*, 232 pp., Longman Science & Technical, Essex.
- Buczowski, D. L. (2006). Kinematic analysis of radial structures around Irnini Mons, Venus. *Journal of Structural Geology*, 28, 2156–2168.
- Campbell, B. A. (1999). Surface formation rates and impact crater densities on Venus. *Journal of Geophysical Research-Planets*, 104, 21,951–21,955.
- Campbell, B. A., Campbell, D. B., Morgan, G. A., Carter, L. M., Nolan, M. C., & Chandler, J. F. (2015). Evidence of crater ejecta on Venus tessera terrain from Earth-based radar images. *Icarus*, 250, 123–130, <https://doi.org/10.1016/j.icarus.2014.11.025>

1116 Campbell, D. B., Stacy, N. J. S., Newman, W. I., Arvidson, R. E., Jones, E. M., Musser, G. S.,  
 1117 Roper, A. Y., Schaller, C. (1992). Magellan observations of extended impact crater related  
 1118 features on the surface of Venus. *Journal of Geophysical Research-Planets*, 97, 16249–  
 1119 16277.  
 1120 Collins, G. C., Head, J. W., Basilevsky, A. T., Ivanov, M. A. (1999). Evidence for rapid regional  
 1121 plains emplacement on Venus from the population of volcanically embayed impact craters.  
 1122 *Journal of Geophysical Research-Planets*, 104, 24121–24139.  
 1123 Compton, R. R. (1985). *Geology in the Field*, 398 pp., John Wiley & Sons, New York, NY.  
 1124 Copp, D. L., Guest, J. E., Stofan, E. R. (1998). New Insights into Coronae evolution: Mapping  
 1125 on Venus. *Journal of Geophysical Research*, 103, 19401–19417.  
 1126 Crumpler, L. S., Aubele, J. C., Senske, D. A., Keddle, S. T., Magee, K. P., Head, J. W. (1997).  
 1127 Volcanoes and centers of volcanism on Venus, in Bouger, S.W., Hunten, D.M., and  
 1128 Phillips, R.J., eds., *Venus II—Geology, geophysics, atmosphere, and solar wind*  
 1129 *environment: Tucson, University of Arizona Press*, p. 697–756.  
 1130 Cushing, G. E., Okubo, C. H. and Titus, T. N. (2015). Atypical pit craters on Mars. New insights  
 1131 from THEMIS, CTX, and HiRISE observations. *Journal of Geophysical Research-Planets*,  
 1132 120, doi: 10.1002/2014JE004735  
 1133 DeLaughter, J. E. and Jurdy, D. M. (1999). Corona classification by evolutionary age. *Icarus*,  
 1134 139, 81–92.  
 1135 DeShon, H. R., Young, D. A., and Hansen, V. L. (2000). Geologic evolution of southern Rusalka  
 1136 Planitia, Venus. *Journal of Geophysical Research-Planets*, 105, 6983–6995.  
 1137 Ferrill, D. A., Wyrick, D. Y., Morris, A. P., Sims, D. W., and Franklin, N. M. (2004). Dilational  
 1138 fault slip and pit chain formation on Mars. *GSA Today*, 14, 1–9.  
 1139 Ford, J. P., Plaut, J. J., Weitz, C. M., Farr, T. G., Senske, D. A., Stofan, E. R., Michaels, G.,  
 1140 Parker, T. J. (1993). Guide to Magellan image interpretation. *National Aeronautics and*  
 1141 *Space Administration Jet Propulsion Laboratory Publication*, 148 p.  
 1142 Ghent, R. R., and Hansen, V. L. (1999). Structural and kinematic analysis of eastern Ovda Regio,  
 1143 Venus: Implications for crustal plateau formation: *Icarus*, 139, 116–136.  
 1144 Gilbert, G. K., 1886, Inculcation of the scientific method: *American Journal Science*, v. 31, p.  
 1145 284–299.  
 1146 Gilmore, M. S., Collins, G. C., Ivanov, M. A., Marinangeli, L., and Head, J. W. (1998). Style and  
 1147 sequence of extensional structures in tessera terrain, Venus. *Journal of Geophysical*  
 1148 *Research-Planets*, 103, 16813–16840.  
 1149 Gregg, T. K. P., and Greely, R. (1993). Formation of Venusian canali: Considerations of lava  
 1150 types and their thermal behaviors. *Journal of Geophysical Research-Planets*, 98, 10873–  
 1151 10882.  
 1152 Grindrod, P. M., and Guest, J. E. (2006). 1:1.5,000,000 Geological map of the Aglaonice region  
 1153 on Venus. *Journal Maps*, 2006, 103–117, doi:10.4113/jom.2006.57  
 1154 Grosfils, E. B., and Head, J. W. (1994). The global distribution of giant radiating dike swarms on  
 1155 Venus: Implications for the global stress state. *Geophysical Research Letters*, 21, 701–704.  
 1156 Guest, J. E., Bulmer, M. H., Aubele, J. C., Beratan, K., Greely, R., Head, J. W., Michaels, G.,  
 1157 Weitz, C., Wiles, C. (1992). Small volcanic edifices and volcanism in the plains on Venus.  
 1158 *Journal of Geophysical Research-Planets*, 97, 15949–15966.  
 1159 Guest, J. E., and Stofan, E. R. (1999). A new view of the stratigraphic history of Venus. *Icarus*.  
 1160 139, 55–66.

1161 Hansen, V. L. (1992). Regional non-coaxial deformation on Venus: Evidence from western  
 1162 Itzpapalotl tessera: *Abstracts of the 23th Lunar and Planetary Science Conference*.  
 1163 Houston, TX.  
 1164 Hansen, V. L. (2000). Geologic mapping of tectonic planets. *Earth and Planetary Science*  
 1165 *Letters*. 176, 527–542.  
 1166 Hansen, V. L. (2005). Venus's shield-terrain. *Geological Society of America Bulletin*. 117, 808–  
 1167 822.  
 1168 Hansen, V. L. (2006). Geologic constraints on crustal plateau surface histories, Venus: The lava  
 1169 pond and bolide impact hypotheses. *Journal of Geophysical Research-Planets*. 111, no.  
 1170 E11010, doi:10.1029/2006JE002714.  
 1171 Hansen, V. L. (2009). Geologic map of the Niobe Planitia quadrangle (V-23), Venus: U.S.  
 1172 *Geological Survey Scientific Investigations Map* 3025, 1:5M,  
 1173 <https://pubs.er.usgs.gov/publication/sim3025>  
 1174 Hansen, V. L. (2018). Global tectonic evolution of Venus. *Philosophical Transactions of the*  
 1175 *Royal Society A*. 376: 20170412. <http://dx.doi.org/10.1098/rsta.2017.0412>.  
 1176 Hansen, V. L., and DeShon, H. R. (2002). Geologic map of the Diana Chasma quadrangle (V-  
 1177 37), Venus: U.S. *Geological Survey Scientific Investigations Map* 2752, 1:5M,  
 1178 <https://pubs.usgs.gov/imap/i2752>  
 1179 Hansen, V. L., and López, I. (2010). Venus records a rich early history. *Geology*. 38, 311–314,  
 1180 doi:10.1130/G30587.1.  
 1181 Hansen, V. L., and López, I. (2018). Mapping of geologic structures in the Niobe-Aphrodite map  
 1182 area of Venus: unraveling the history of tectonic regime change. *Journal of Geophysical*  
 1183 *Research-Planets*. 123, 1760–1790.  
 1184 Hansen, V.L., and López, I. (2020). Geologic Map of Aphrodite Map Area (AMA; I-2476),  
 1185 Venus. Preprint on <https://doi.org/10.1002/essoar.10502475.1>  
 1186 Hansen, V. L., and Olive, A. (2010). Artemis, Venus: The largest tectonomagmatic feature in the  
 1187 solar system? *Geology*. 38, 467–470, doi:10.1130/G30643.1.  
 1188 Hansen, V. L., Phillips, R. J., Willis, J. J., and Ghent, R. R. (2000). Structures in tessera terrain,  
 1189 Venus: Issues and answers. *Journal of Geophysical Research-Planets*. 105, 4135–4152.  
 1190 Hansen, V. L., and Tharalson, E. R. (2014). Geologic map of the Agnesi quadrangle (V-45),  
 1191 Venus: *U.S. Geological Survey Scientific Investigations Map* 3250, 1:5M,  
 1192 <https://pubs.er.usgs.gov/publication/sim3250>  
 1193 Hansen, V. L., and Willis, J. J. (1996). Structural analysis of a sampling of tesserae: Implications  
 1194 for Venus geodynamics. *Icarus*. 123, 296–312.  
 1195 Hansen, V. L., and Willis, J. J. (1998). Ribbon terrain formation, southwestern Fortuna Tessera,  
 1196 Venus—Implications for lithosphere evolution. *Icarus*. 132, 321–343.  
 1197 Hansen, V. L., and Young, D. A. (2007). Venus's evolution: A synthesis, in Cloos, M., Carlson,  
 1198 W.D., Gilbert, M.C., Liou, J.G., and Sorensen, S.S., eds., *Convergent margin terranes and 6*  
 1199 *associated regions—A Tribute to W.G. Ernst: Geological Society of America*, p. 255–273,  
 1200 10.1130/2006.2419(13).  
 1201 Hauck, S. A., Phillips, R. J., and Price, M. H. (1998). Venus: Crater distribution and plains  
 1202 resurfacing models. *Journal of Geophysical Research-Planets*. 103, 13635–13642.  
 1203 Herrick, R. R., and MacGovern, P. J. (2000). Kunhild and Ereshkigal, an extinct hot-spot región  
 1204 on Venus. *Geophysical Research Letters*. 27, 839–842.  
 1205 Herrick, R. R., and Sharpton, V. L. (2000). Implications from stereo-derived topography of  
 1206 Venusian impact craters. *Journal of Geophysical Research-Planets*. 105, 20245–20262.

1207 Herrick, R. R., and Rumpf, M. E. (2011). Post-impact modification by volcanic or tectonic  
 1208 processes as the rule, not the exception, for Venusian craters. *Journal of Geophysical*  
 1209 *Research–Planets*. 116, no. E02004, doi:10.1029/2010JE003722.  
 1210 Herrick, R. R., Sharpton, V. L., Malin, M. C., Lyons, S. N., and Feely, K. (1997). Morphology  
 1211 and morphometry of impact craters, in Bouger, S.W., Hunten, D.M., and Phillips, R.J.,  
 1212 eds., *Venus II: Tucson*, University of Arizona Press, p. 1015–1046.  
 1213 Ivanov, M. A., and Head, J. W. (1996). Tessera terrain on Venus: A survey of the global  
 1214 distribution, characteristics, and relation to surrounding units from Magellan data. *Journal*  
 1215 *of Geophysical Research–Planets*, 101, 14861–14908.  
 1216 Ivanov, M. A., and Head, J. W. (2015a). Volcanically embayed craters on Venus: testing the  
 1217 catastrophic and equilibrium resurfacing models. *Planetary and Space Science*. 106, 116–  
 1218 121.  
 1219 Ivanov, M. A., and Head, J. W. (2015b). The history of tectonism on Venus: A stratigraphic  
 1220 analysis. *Planetary and Space Science*. 113–114, 10–32.  
 1221 Izenberg, N. R., Arvidson, R. E., and Phillips, R. J. (1994). Impact crater degradation on  
 1222 Venusian plains. *Geophysical Research Letters*. 21, 289–292.  
 1223 Jones, A. P., and Pickering, K. T. (2003). Evidence for aqueous fluid-sediment transport and  
 1224 erosional processes on Venus. *Journal Geological Society of London*. 160, 319–327.  
 1225 Kirk, R. L., and Chadwick, D. J. (1994) Splotches on Venus: distribution, properties and  
 1226 classification. *Abstracts of the 25th Lunar and Planetary Science Conference*. Houston,  
 1227 TX, 14–18 March 1994., p.705.  
 1228 Kirk, R. L., Soderblom, L., and Lee, E. (1992). Enhanced visualization for interpretation of  
 1229 Magellan radar data—Supplement to the Magellan special issue. *Journal of Geophysical*  
 1230 *Research–Planets*. 97, 16371–16380.  
 1231 Kreslavsky, M. A., Ivanov, M. A., and Head, J. W. (2015). The resurfacing history of Venus:  
 1232 Constraints from buffered crater densities. *Icarus*. 250, 438–450.  
 1233 Komatsu, G., and Baker, V. R. (1994). Meander properties of venusian channels. *Geology*. 22,  
 1234 67–70.  
 1235 Lang, N. P., and Hansen, V. L. (2006). Venusian channel formation as a subsurface process.  
 1236 *Journal of Geophysical Research–Planets*. 111, doi:10.1029/2005JE002629.  
 1237 Lang, N. P., and Hansen, V. L. (2008). Geologic map of the Green- away quadrangle (V–24),  
 1238 Venus: U.S. Geological Survey Scientific Investigations Map 3089, scale 1:5,000,000  
 1239 [<http://pubs.usgs.gov/sim/3089>].  
 1240 López, I. (2011). Embayed intermediate volcanoes on Venus: Implications for the evolution of  
 1241 the volcanic plains. *Icarus*. 213, 73–85.  
 1242 Maltman A. (1990). *Geological Maps: An Introduction*. Open University Press, Buckingham  
 1243 U.K., 184 pp.  
 1244 McGill, G. E., and Campbell, B. A. (2004). Ages of Venusian ridge belts relative to regional  
 1245 plains. *Lunar and Planetary Science Conference XXXVI*. Houston, Tex., abstract #1143.  
 1246 McKinnon, W. B., Zahnle, K. J., Ivanov, B. A., and Melosh, H. J. (1997). Cratering on Venus:  
 1247 Models and observations, in Bouger, S.W., Hunten, D.M., and Phillips, R.J., eds., *Venus II:*  
 1248 *Tucson*, University of Arizona Press, p. 969–1014.  
 1249 Okubo, C. H., and Martel, S. J. (1998). Pit crater formation on Kilauea volcano, Hawaii. *Journal*  
 1250 *of Volcanology and Geothermal Research*. 86, 1–8.  
 1251 O’Rourke, J. G., and Korenaga, J. (2015). Thermal evolution of Venus with argon degassing.  
 1252 *Icarus*. 260, 128–140.

1253 Pavri, B., Head, J. W., Klose, K. B., and Wilson, L. (1992). Steep-sided domes on Venus:  
 1254 Characteristics, geologic setting, and eruption conditions from Magellan data. *Journal of*  
 1255 *Geophysical Research-Planets*. 97, 13445-13478.

1256 Phillips, R. J., and Hansen, V. L. (1994). Tectonic and magmatic evolution of Venus. *Annual*  
 1257 *Reviews of the Earth and Planetary Sciences*. 22, 597-654.

1258 Phillips, R. J., and Hansen, V. L. (1998). Geological evolution of Venus: Rises, plains, plumes  
 1259 and plateaus. *Science*. 279, 1492-1497.

1260 Phillips, R. J., and Izenberg, N. R. (1995). Ejecta correlations with spatial crater density and  
 1261 Venus resurfacing history. *Geophysical Research Letters*. 22, 1517-1520.

1262 Phillips, R. J., Raubertas, R. F., Arvidson, R. E., Sarkar, I. C., Herrick, R. R., Izenberg, N.,  
 1263 Grimm, R. E. (1992). Impact crater distribution and the resurfacing history of Venus.  
 1264 *Journal of Geophysical Research-Planets*. 97, 15923-15948.

1265 Price, M., & Suppe, J. (1995). Constraints on the resurfacing history of Venus from the  
 1266 hypsometry and distribution of volcanism, tectonism, and impact craters. *Earth, Moon, and*  
 1267 *1570 Planets*, 71(1-2), 99-145. <https://doi.org/10.1007/BF00612873>

1268 Reese, C. C., Solomatov, V. S., and Orth, C. P. (2007). Mechanisms for cessation of magmatic  
 1269 resurfacing on Venus. *Journal of Geophysical Research-Planets*, 112, E04S04,  
 1270 doi:10.1029/2006JE002782.

1271 Romeo, I. (2013). Monte Carlo models of the interaction between impact cratering and volcanic  
 1272 resurfacing on Venus: the effect of the Beta-Atla-Themis anomaly. *Planetary Space*  
 1273 *Science*. 87, 157-172.

1274 Romeo, I., and Turcotte, D. L. (2010). Resurfacing on Venus. *Planetary Space Science*. 58,  
 1275 1374-1380, doi:10.1016/j.pss.2010.05.022.

1276 Ruiz, J. (2007). The heat flow during formation of ribbon terrains on Venus. *Planetary and*  
 1277 *Space Science*, 55, 2063-2070, doi:10.1016/j.icarus.204.11.007.

1278 Sandwell, D. T., Johnson, C. L., Bilotti, F., and Suppe, J. (1997). Driving forces for limited  
 1279 tectonics on Venus. *Icarus*. 129, 232-244, doi: 10.1006/icar.1997.5721.

1280 Schaber, G. G., Strom, R. G., Moore, H. J., Soderblom, L. A., Kirk, R. L., Chadwick, D. J.,  
 1281 Dawson, D. D., Gaddis, L. R., Boyce, J. M., Russell, J. (1992). Geology and distribution of  
 1282 impact craters on Venus: What are they telling us? *Journal of Geophysical Research-*  
 1283 *Planets*, 97, 13257-13302.

1284 Schultz, R. A., Okubo, C. H., Goudy, C. L., and Wilkins, S. J. (2004). Igneous dikes on Mars  
 1285 revealed by Mars Orbiter Laser Altimeter topography. *Geology*. 32, 889-892.

1286 Senske, D. A., Schaber, G. G., and Stofan, E. R. (1992). Regional topographic rises on Venus:  
 1287 Geology of Western Eistla Regio and comparison to Beta Regio and Atla Regio. *Journal of*  
 1288 *Geophysical Research-Planets*, 97, 13395-13420.

1289 Shalygin, E. V., Markiewicz, W. J., Basilevsky, A. T., Titov, D. V., Ignatiev, N. I., Head, J. W.  
 1290 (2015). Active volcanism on Venus in the Ganiki Chasma rift zone. *Geophysical Research*  
 1291 *Letters*. 42, 4762-4769.

1292 Shankar, B. (2008). A global survey of circular lows: A subset of Coronae, Venus, University of  
 1293 Minnesota Duluth, M.S. Thesis, 87 pp.

1294 Skinner, J. A., and Tanaka, K. L. (2003) How should map units be defined? *Lunar and Planetary*  
 1295 *Science Conference XXXIV*. Houston, Tex., abstract #2100.

1296 Smrekar, S. E., and Stofan, E. R. (1999) Origin of corona-dominated topographic rises on Venus.  
 1297 *Icarus*. 139, 100-116.



1298 Solomatov, V. S., and Moresi, L. N. (1996). Stagnant lid convection on Venus. *Journal of*  
1299 *Geophysical Research*. 101, 4737–4753, doi:10.1029/95JE03361.

1300 Stofan, E. R., Sharpton, V. L., Schubert, G., Baer, G., Bindschadler, D. L., Janes, D. M., and  
1301 Squyres, S. W. (1992). Global distribution and characteristics of coronae and related  
1302 features on Venus: Implications for origin and relation to mantle processes. *Journal of*  
1303 *Geophysical Research-Planets*. 97, 13347–13378.

1304 Stofan, E. R., Brian, A. W., and Guest, J. E. (2005) Resurfacing styles and rates on Venus:  
1305 Assessment of 18 Venusian quadrangles. *Icarus*. 173, 312–321.

1306 Stofan, E. R., Anderson, S. W., Crown, D. A., and Plaut, J. J. (2000) Emplacement and  
1307 composition of steep-sided domes on Venus. *Journal of Geophysical Research-Planets*.  
1308 105, 26757–26771.

1309 Stofan, E. R., Senske, D. A., and Michaels, G. (1993). Tectonic features in Magellan data, in  
1310 Ford, P.J., Plaut, J., Wietz, C.M., and 5 others, eds., Guide to Magellan image  
1311 interpretation: Pasadena, Calif., National Aeronautics and Space Administration Jet  
1312 Propulsion Laboratory, p. 93–108.

1313 Strom, R. G., Schaber, G. G., and Dawson, D. D. (1994). The global resurfacing of Venus.  
1314 *Journal of Geophysical Research-Planets*. 99, 10899–10926.

1315 Tanaka, K. L., Skinner, J. A., Hare, T. M. (2010). Planetary Geologic Mapping Handbook. U.S.  
1316 Geological Survey.

1317 Tanaka, K. L., Schaber, G. G., Chapman, M. G., Stofan, E. R., Campbell, D. B. Davis, P. A.,  
1318 Guest, J. E., McGill, G. E., Rogers, P. G., Saunders, R. S. and Zimbelman, J. R. (1993).  
1319 The Venus geologic mappers' handbook (2nd ed.): U.S. Geological Survey Open-File  
1320 Report 94–438, 68 p.

1321 Turcotte, D. L. (1993). An episodic hypothesis for Venusian tectonics. *Journal of Geophysical*  
1322 *Research-Planets*, 98, 17061–17068.

1323 Turcotte, D. L., Morein, G., and Malamud, B. D. (1999) Catastrophic resurfacing and episodic  
1324 subduction on Venus. *Icarus*. 139, 49–54.

1325 Waltham, D., Pickering, K. T., and Bray, V. J. (2008). Particulate gravity currents on Venus.  
1326 *Journal of Geophysical Research-Planets*. 113, E02012, doi:10.1029/2007JE002913.

1327 Watters, T. R. (1988). Wrinkle ridge assemblages on the terrestrial planets. *Journal of*  
1328 *Geophysical Research-Planets*. 93, 236–254.

1329 Weitz, C. M. (1993). Impact craters, in Ford, P.J., Plaut, J., Wietz, C.M., and 5 others, eds.,  
1330 Guide to Magellan image interpretation: Pasadena, Calif., National Aeronautics and Space  
1331 Administration Jet Propulsion Laboratory, p. 75–92.

1332 Wilhelms, D. E. (1990). Geologic mapping, in Greeley, R., and Batson, R.M., eds., Planetary  
1333 mapping. New York, Cambridge University Press, p. 208–260.

1334 Wilhelms, D. E. (1972). Geologic mapping of the second planet. *U.S. Geological Survey*  
1335 *Interagency Report*, Astrogeology, 55 pp.

1336 Williams-Jones, G., Williams-Jones, A. E., and Stix, J. (1998). The nature and origin of venusian  
1337 canali. *Journal of Geophysical Research-Planets*. 103, 8545–8555.

1338 Whitten J. L., & Campbell, B. A. (2016). Recent volcanic resurfacing of Venusian craters.  
1339 *Geology*, 44, 519–522.

1340 Young, D. A., and Hansen, V. L. (2003). Geologic map of the Rusalka Planitia Quadrangle (V-  
1341 25), Venus. *U.S. Geological Survey Scientific Investigations Map* I-2783,  
1342 <http://pubs.usgs.gov/imap/i2783/>

Young, D. A., and Hansen, V. L. (2005). Poludnista Dorsa, Venus: History and context of a deformation belt. *Journal of Geophysical Research-Planets*. 110, doi:10.1029/2004JE002280.

Zimbelman, J. R. (2001). Image resolution and evaluation of genetic hypotheses for planetary landscapes. *Geomorphology*, 37, 179–199.

## Captions to Figures and Tables.

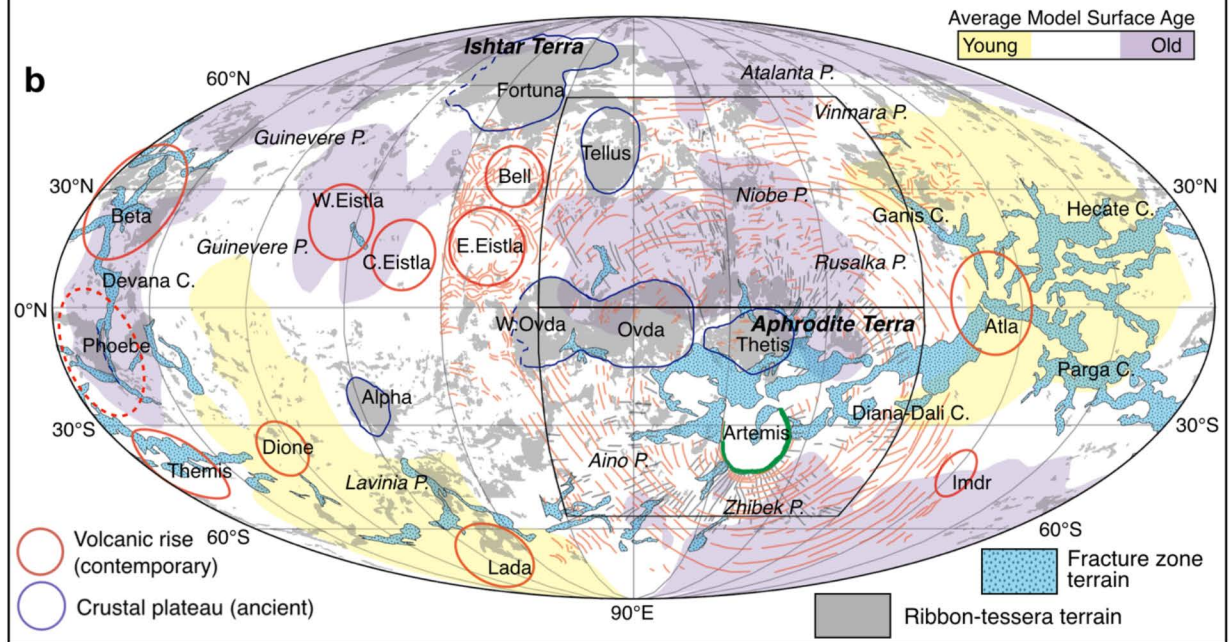
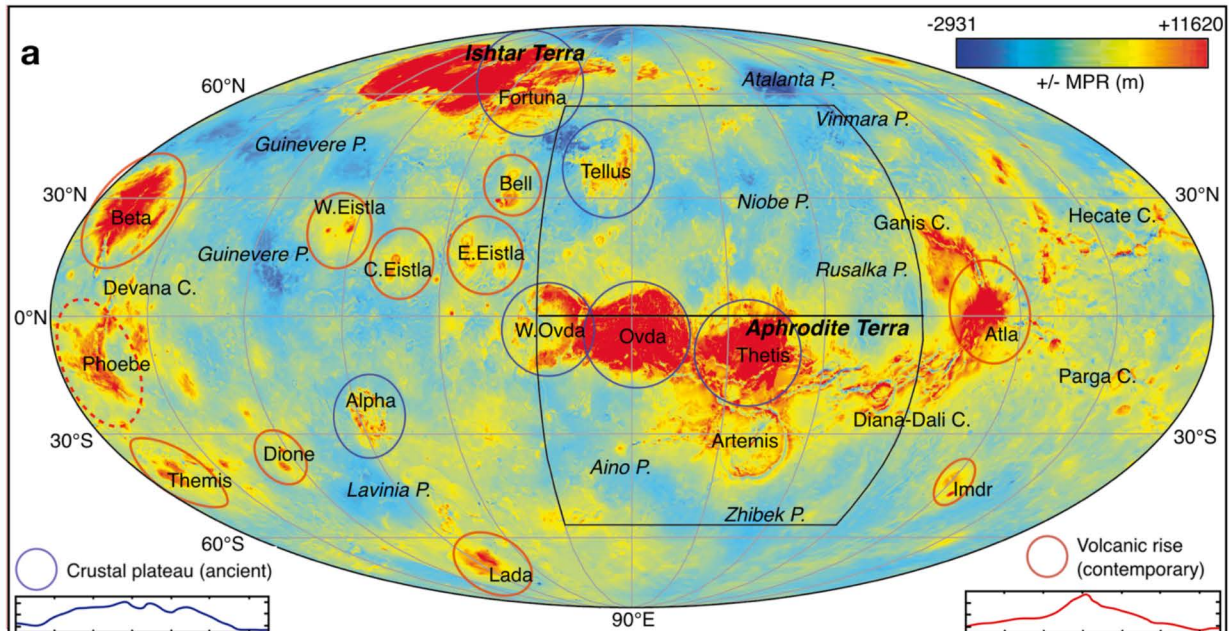
*Figure 1.* Mollweide projections of Venus; the NMA (north) and AMA (south) are shown as polygons. (a) Altimetry: highlands, red; mesolands, yellow; lowlands, blues; Ishtar Terra and Aphrodite Terra are composite highlands; highland features include crustal plateaus and volcanic rises, and hybrid Phoebe Regio. Planitiae are indicated by ‘P.’, chasmata with ‘C.’ Topographic profiles (Ovda Regio, 90°E; Beta Regio 23.6°E), ~6 km vertical, 3500 km horizontal. b) Global distribution of: average model surface age provinces [Phillips & Izenberg, 1995; Hansen & Young, 2007]; fracture zone terrain [‘rift’ of Price & Suppe, 1995]; ribbon-tessera terrain [Hansen & López, 2010]; Artemis Chasma (green); trajectories of Artemis Chasma-radial fractures (gray lines) and wrinkle ridges (faded red lines), including Artemis Chasma-concentric wrinkle ridges and wrinkle ridges not concentric to Artemis [Hansen & Olive, 2010]. Labels as in (a). Modified from Hansen [2018].

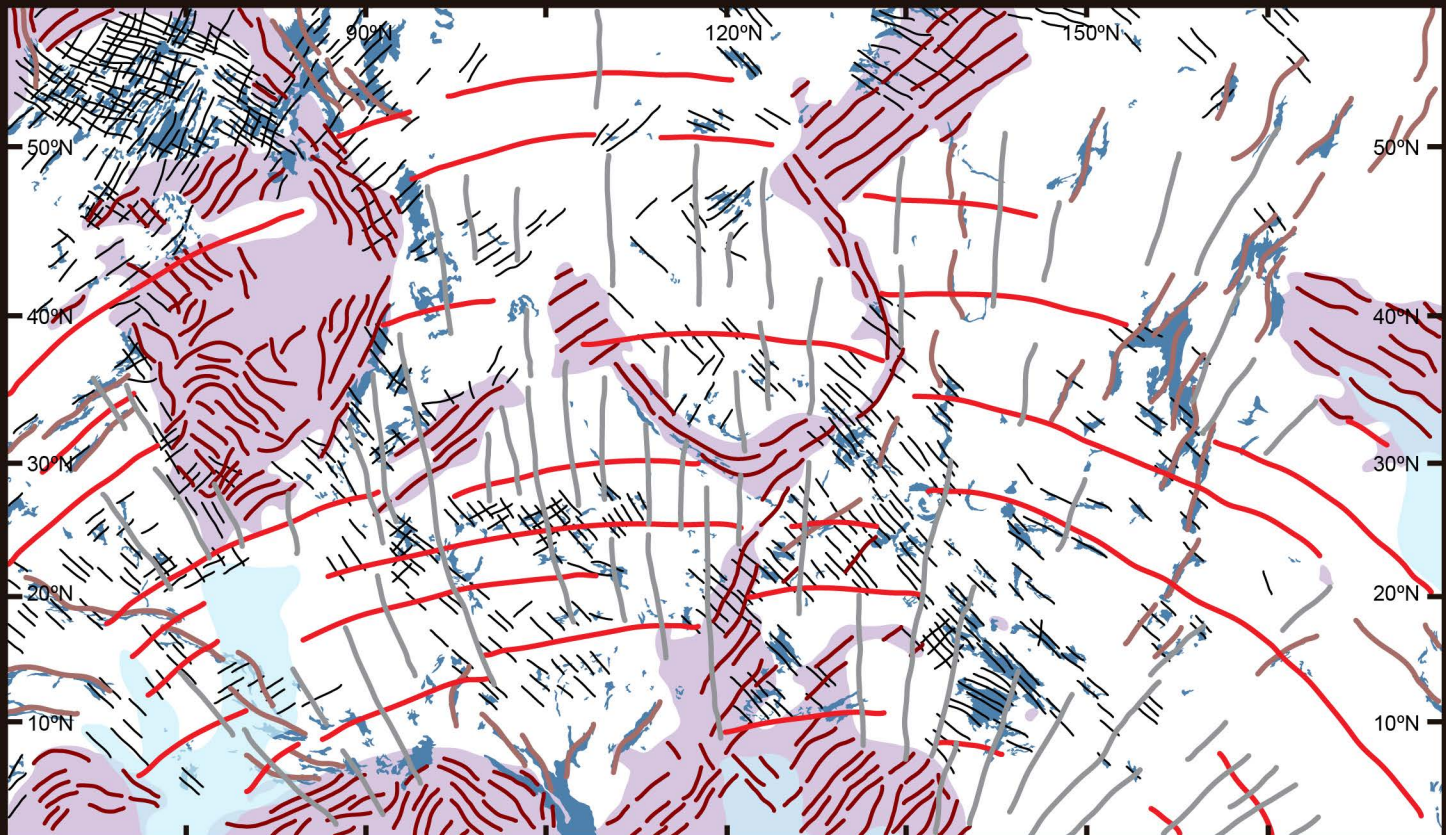
*Figure 2.* Mercator projection summary of the tectonic regimes within the NMA.

*Table 1.* Niobe Region (I-2467) Impact Craters.






*Plate 1.* Geologic Map of the Niobe Planitia Region (I-2467), Venus.








### Ancient Era

-  Deformation belts
-  Tesserae folds
-  NE- & NW-fractures
-  Basal terrain
-  Tessera terrain

### Artemis Superstructure Era

-  Artemis-concentric wrinkle ridge trajectories
-  Artemis-radial structure trajectories

### Fracture Zone Domain Era

-  Fracture Zone Complex

Time



**Table 1. Niobe Region (I-2467) Impact Craters**

Name	Latitude (deg N)	Longitude (deg E)	Diameter (km)	Elevation	Vmap	Units	Ejecta blanket	Impact Halo	Central Peak	Rim	Dark Floor	Crater density	Crater Database	Deformed	Temporal implications
Adivar	8,9	76,2	29	6051.76	22	vmu	Y	70	Y	Y	Y	2,55	H,S?	N	Postdates ACWR formation
Adzoba	12,8	117	12,2	6051.50	23	bst	Y	x	N	Y	N	3,18	H,S	N	Postdates ARF and ACWR formation
Afua	15,5	124	11	6051.45	24	btL, bst	Y	x	N	Y	N	3,18	H,S	Y	
Aimee	16,1	127,2	16,8	6051.09	24	fcA	Y	50	Y?	Y	N	2,86	H,S	N	Postdates ACWR formation
Almeida	46,6	123,3	14,9	6051.92	12	st	Y	140	Y	Y	N	2,86	H,S	N	Postdates ARF formation
Altana*	1,5	69,9	5,7	6053.47	22	rtMa, fcK	Y	x	N	Y	N	2,23	H	N	
Amaya	11,3	89,3	34	6052.56	22	bst, fcOv	Y	120	Y	Y	Y	2,55	H,S	N	Postdates ARF and local radial fractures, with possible later structural reactivation
Anaxandra	44,2	162,3	20,2	6051.31	13	vmu	Y	80	Y	Y	Y	1,59	H,S	N	Postdates ARF, ARF burial and subsequent inversion, and ACWR formation
Antonina	28,1	106,9	11	6050.63	11	vmu	N	60	N	N	N	2,23	H,S	N	Postdates ACWR formation
Anush	14,9	86,5	12,2	6051.88	22	bst	Y	x	Y	Y	Y	1,91	H,S	N	Postdates ACWR formation
Asmik	3,9	166,5	18,6	6051.57	25	fcRu2	Y	130	N	Y	Y?	3,5	H,S	N	Postdates ARF, ARF burial and subsequent inversion, and ACWR formation
Avene	40,4	149,4	11	6051.08	13	vmu	Y	40	N	Y	N	2,55	H,S	N	Postdates ACWR formation
Ban Zhao	17,2	146,9	38,3	6050.80	24	vmu, btL	Y	x	Y	Y	N	2,86	H,S	N	Postdates ACWR formation
Barrera	16,5	109,4	26,8	6051.67	23	bst, st	Y	70	Y	Y	Y	3,18	H,S	N	Postdates ACWR formation
Barto	45,3	146,2	47,9	6051.30	12	vmu	Y	x	Y	Y	Y	3,82	H,S	N	Postdates ACWR formation?
Bernhardt	31,6	84,4	25	6052.02	10	bst	Y	x	Y	Y	Y	2,55	H	N	
Bourke-White	21,2	147,9	34,4	6050.96	24	vmu	Y	120	Y	Y	Y	2,55	H,S	N	Postdates ACWR formation
Budevska	0,5	143,2	18,7	6052.22	24	st	Y	70	Y	Y	N	2,55	H,S	N	Postdates ARF formation
Caccini	17,4	170,4	37,5	6051.68	25	vmu	Y	130	Y	Y	N	1,91	H,S	N	Postdates ACWR formation
Caldwell	23,6	112,5	52	6051.52	23	bst	Y	x	Y?	Y	N	3,18	H,S	N	Postdates ACWR formation
Callirhoe	21,2	140,7	32,9	6051.33	24	st	Y	x	Y	Y	Y	2,55	H,S	N	Postdates NW-fracture formation, although NW-fractures may show local evidence of later reactivation
Carter	5,3	67,3	19,3	6054.13	22	rtMa	Y	55	N	Y	N	2,23	H,S	N	
Cather	47,1	107	26,5	6051.60	11	st?	Y?	x	N	Y	Y	1,27	H,S	N	



Chapelle	6,4	103,8	20,8	6051.86	23	fcOv	Y	x	Y	Y	Y	2,23	S	N	
Christie	28,3	72,7	24,3	6050.84	10	vmu	Y	170	Y	Y	Y	2,55	H,S	N	Postdates ACWR formation
Cochran	51,9	143,4	98,1	6051.77	4	vmu	Y	x	N	Y	Y	3,18	H,S	N	Postdates ACWR formation
Cori	25,4	72,9	54,7	6050.79	10	vmu	Y	x	N	Y	Y	2,86	H,S	N	Postdates ACWR formation
Corpman	0,3	151,8	45,1	6052.21	25	fcOv	Y	110	N	Y	Y	3,5	H,S	N	Postdates ARF formation, although ARF may also been locally reactivated
Datsolalee	38,3	171,8	17	6051.44	13	bst	Y	120	N	Y	N	1,27	H,S	Y?	
de Beauvoir	2	96,1	53,3	6054.79	23	rtO, itbO	Y	x	N	Y	Y	3,82	H,S	N	
Doris	2,3	90	15,5	6055.01	22,23	rtO	Y?	x	N	Y	Y	0	H,S	Y	Predates ARF or local radial fractures
du Chatelet	21,5	165	19	6051.73	25	vmu	Y	60	?	Y	?	1,91	H,S	N	big enough to show?
Erkeley	43,9	103,4	9,3	6051.69	11	vmu	N	x	N	N	N	1,27	H,S	N	
Escoda	18,2	149,5	19,5	6051.12	24	vmu, fcl	Y	x	N	Y	Y	2,23	H,S	N	Postdates ACWR formation
Estelle	1,1	93,7	17,8	6055.06	23	rtO, itbO	Y?	x	Y	Y	N	3,5	H,S	N	
Faiga	4,9	170,9	10,6	6051.48	25	fcRu2	Y	70	N	Y	N	3,5	H,S	N	
Fazu	32,4	106	7,1	6050.75	11	vmu	Y	60	N	Y	N	1,91	H,S	N	
Ferrier	15,7	111,3	29	6051.51	23	bst	Y	x	Y	Y	Y	3,18	H,S	N	Crater may postdate ARF formation, but ARF may have been locally reactivated after crater formation
Fiona	5	166,6	5	6051.40	25	fcRu2	Y	30	N	Y	N	3,5	H,S	N	
Firuzi	51,8	108	4,9	6051.50	3	bst	Y	x	N	Y	N	0	H,S	N	
Frosya	29,5	113,4	9,6	6050.87	11	vmu	Y	50	N	Y	N	3,5	H,S	N	Postdates ACWR formation
Greenaway	22,9	145,1	92,3	6051.28	24	btLI, st, vmu	Y	x	N	Y	N	2,55	H,S	N	Postdates ACWR formation
Gregory	7,1	95,8	18	6053.17	23	bst	Y	x	N	Y	N	3,18	H,S	N	Postdates ARF formation
Hannah	17,9	102,6	19,1	6051.54	23	st	Y	x	Y	Y	Y?	2,55	H,S	N	Postdates ACWR formation
Helvi	12,4	82,7	11,2	6052.35	22	bst	Y	x	N	Y	N	2,55	H,S	N	Postdates ARF formation
Hepworth	5,1	94,6	62,5	6054.16	23	rtO, itbu	Y	x	N	Y	Y	3,5	H,S	N	
Himiko	19	124,3	36,7	6051.42	24	fcA, bst	Y	x	Y	Y	N	2,86	H,S	N	Postdates ARF and AWCR formation, and formation of concentric fractures of Abundia Corona and the steep sided dome
Horner	23,4	97,8	24,7	6051.36	23	bst, fcOv	Y	x	Y	Y	Y	2,86	H,S	N	Postdates formation of concentric fractures of Maya Corona
Hwangcini	6,3	141,7	30,8	6051.73	24	st	Y	230	Y	Y	Y	2,55	H,S	N	Postdates ARF formation
Icheko*	6,6	97,9	5,6	6053.53	23	bst	Y	x	N	Y	N	2,86	H,S	N	Postdates tessera ribbon fabric formation, but may be deformed by reactivation of ribbon structures?

Iraida*	27,8	108	6	6050.65	11	vmu	Y	x	N	Y	N	1,91	H	N	Postdates ARF, ARF burial and subsequent inversion as WRs
Irene	49,8	134	13,5	6052.15	12	rtA, st	Y	x	N	Y	N	4,14	H,S	Y?	
Irina	34,9	91,2	14,2	6051.47	11	st	Y	x	N	Y	Y	1,59	H,S	N	Postdates ACWR formation
Irinuca*	51,4	121,9	8,1	6051.80		fmJ	Y	x	N	Y	N	2,23	H,S	N	
Jaantje	46,5	123,1	7,3	6051.98		st	Y	140	N	Y	N	2,86	H,S	N	Postdates ARF formation
Jamila	45,8	134,7	7,8	6051.72	12	vmu	Y	50	N	Y	N	3,5	H,S	N	Postdates ACWR formation
Khadako	54,2	139,4	7	6051.95	4	itbu	Y?	x	N	Y	Y	2,86	H,S	Y?	Posts formation or reactivation of NE and NW-trending fractures
Khatun	40,3	87,2	42,4	6052.55	10	rtT	Y	120	Y	Y	Y	1,27	H,S	N	
Kiris	20,9	98,8	13,3	6051.67	23	bst	Y	x	N	Y	N	2,23	H,S	N	Postdates formation of NW-trending fractures and ARF, but these fracture suites may have been reactivated after crater formation
Kollwitz	25,2	133,6	28,9	6051.23	12	btLI, bst, vmu	Y	x	Y	Y	Y	1,27	H,S	N	
Konopnicka	14,5	166,6	19,9	6051.74	25	vmu	Y	60	Y	Y	Y	2,55	H,S	N	
Kylii	41,1	67	12,8	6051.46	10	bst	Y	x	Y	Y	N	1,59	H,S	N	
Laura	48,9	141,2	18,4	6051.46	12	vmu	Y	x	N	Y	N	3,82	H,S	N	Temporal relations between crater and WRs unclear due to spacing of wrinkle ridges, low strain, and radar brightness of both ejecta and WRs
Li Quingzhao	23,7	94,6	22,4		23	bst		x	Y	Y	N	2,55	H,S	N	Crater postdates formation of NW-trending fractures
Lullin	23	81,3	24,9	6051.80	22	bst, fcKu2	Y	160	Y	Y	Y	2,86	H,S	N	Postdates ACWR formation
MacDonald	30	120,7	18,4	6051.70	12	st	Y	90	N	1	Y?	1,59	H,S	N	Postdates ACWR formation
Manzolini	25,7	91,3	43,7	6051.67	11	bst, st	Y	x	Y	Y	Y	2,55	H,S	N	Predates ARF
Maranda	4,9	169,7	17,1	6051.53	25	fcRu2	Y	x	Y	Y	Y?	3,5	H,S	Y?	Predates local radial fractures
Marere*	19,6	65,8	6,7	6051.15	22	vmu	Y	x	N	Y	N	2,23	H,S	N	
Maria Celeste	23,4	140,4	96,6	6051.38	24	vmu, st	Y	x	N	Y	Y	2,86	H,S	N	Temporal relations with WRs difficult to robustly constrain given the presence of extensive halo deposits
Marysya*	53,3	75,1	6,9	6051.39	3	btu	Y?	x	N	Y	N	1,91	H,S	Y	
Mbul'di*	23,8	74,7	5,5	6050.73	22	vmu	Y	x	N	Y	N	2,86	H,S	N	Postdates ACWR formation
Merian	34,5	76,2	21,9	6052.88	10	rtT	Y?	x	?	Y	N	1,59	H,S	Y	
Merit Ptah	11,4	115,6	17	6051.19	23	bst	N	x	N	N	N	2,86	H,S	N	Postdates formation of NW-trending fractures at this location
Millay	24,4	111,3	48,3	6051.33	23	bst	Y	x	Y	Y	Y	2,86	H,S	N	Postdates ACWR formation

Mosaido	17,3	75,2	7,3	6051.59	22	bst	Y	x	N	Y	N	3,5	H,S	N	Postdates ACWR formation
Moses	34,6	119,9	28,1	6051.09	11	bst, st	Y	x	Y	Y	Y	2,23	H,S	N	Postdates ACWR formation
Mu Guiying	41,2	81,1	32,7	6051.60	10	bst	Y	x	Y	Y	N	1,59	H,S	N	
Nana	49,8	75,4	8,3	6051.35	10	st	Y	x	N	Y	N	1,59	H,S	N	
Naomi	6	70,3	17,1	6053.07	22	rtMa, bst	Y?	x	N	Y	N	2,55	H,S	Y	Predates formation of radial fractures associated with Kaltash Corona?
Neeltje	12,4	124,5	10,3	6051.27	24	btL	N	x	?	Y	?	4,14	H,S	N	
Nemcova	5,9	125,1	21,4	6052.47	24	fcRo	Y	90	Y	Y	Y	1,91	H,S	N	Postdate formation of radial fractures associated with Rosmerta Corona
Nijinskaya	25,8	122,5	35,4	6051.09		vmu, bst	Y	x	Y	Y	Y	2,55	H,S	N	
Nsele*	6,7	64,2	4,9	6053.50	22	vmu	Y?	40	N	Y	N	2,23	H,S	N	
Nyal'ga*	17	64,5	5,2	6051.49	22	vmu	Y?	x	N	Y	N	1,59	H,S	N	
Odarka	40,7	138,2	7,2	6051,6	12	vmu	Y	70	N	Y	N	2,55	H,S	N	Postdates ACWR formation
Ogulbek*	2,4	145,1	6,6	6052.29	24	bst	Y?	70	N	Y	N	2,86	H	N	Postdates formation of ARF
Olena*	10,9	149	7	6051.42	22	bst	Y	x	N	Y	N	2,55	H,S	N	Postdates formation of local WR formation
Ortensia	7,6	155,7	6,6	6051.78	25	fsL	Y	50	N	Y	N	1,91	H,S	N	
Oshalche	29,7	155,5	9,6	6050.91	13	vmu	Y	x	N	Y	Y?	0,64	H,S	N	
Parra	20,5	78,5	42,8	6052.02	22	fcKu2	Y	140	N	Y	N	3,5	H,S	N	
Pasha	42,7	156,3	7,6	6050.66		vmu	Y	50	N	Y	N	2,55	H,S	N	Postdates ACWR formation
Phyllis	12,2	132,4	10,6	6051.74	24	bst, st	Y	130	N	Y	N	2,55	H,S	N	Postdates ARF formation
Polina	42,4	148,2	20,5	6051.18	11	vmu	Y	130	N	Y	N	2,86	H,S	N	
Puhioia*	20,6	69,4	6,4	6051.02	22	vmu	Y?	x	N	Y	N	0	H,S	N	
Qulzhan	23,5	165,4	10,8	6051.33	25	vmu	Y	140	N	Y	N	1,59	H,S	N	Postdates ACWR formation
Quslu	6,2	166,8	8,6	6051.34	25	fcRU2	Y	x	Y	Y	N	3,18	H,S	N	Postdates formation of ARF and ACWR
Rampyari	50,6	179,3	6	6050.75	4	vmu	Y	80	N	Y	Y	2,23	H	N	Postdates ACWR formation
Regina	30	147,3	25,5	6051.35	12	bst	Y	220	Y	Y	Y	1,59	H,S	N	
Riley	14	72,5	18,8	6051.91	22	fmU1	Y	80	Y	Y	Y?	2,86	H,S	N	
Romanskaya	23,2	178,5	31,7	6052.18	25	fRk	Y	80	Y?	Y	Y	0,95	H,S	Y	
Rowena	10,4	171,4	19,6	6051.48	25	fcRu2	Y	x	Y	Y	Y	3,82	H,S	N	Postdates WR formation
Surija	5,3	178,2	14,5	6051.36	25	vmu	Y	130	Y	Y	N	2,23	H,S	N	
Susanna	6	93,3	13,2	6053.37	23	fcOv	Y	71	N	Y	N	3,5	H,S	N	Postdates ARF formation
Taglioni	41,7	122,6	31	6051.47	12	bst	Y	90	Y	Y	Y	1,59	H,S	N	
Tahia*	44,2	73,7	9,1	6050.70	10	bst	Y	x	N	Y	N	2,55	H	N	

Tekarohi	21,2	76,5	8,9	6051.69	22	bst	Y	x	N	Y	N	2,86	H,S	N	Likely postdates ARF formation, but affected by local reactivation of ARF
Tinyl	9,7	132,1	11,7	6051.49	24	bst	Y	x	N	Y	N	2,55	H,S	Y	
Tseraskaya	28,6	79,3	30,1	6051.64	10	rtT	Y	x	Y	Y	Y	2,86	H,S	N	
Tsiala*	2,9	100	16	6054.83	23	rtO	Y?	x	N	Y	N	3,82	H,S	N	Postdates ACWR formation
Ualinka	13,2	168,6	8,1	6051.97	25	vmu	Y	x	N	Y	N	2,86	H,S	N	
Udyaka	30,8	172,9	12,2	6051.36	13	vmu	Y	130	N	Y	N	1,59	H,S	N	
Unay	53,5	172,6	10,8	6050.83	4	vmu	Y	40	N	Y	N	1,59	H,S	N	
unnamed*	5,8	84,3	5,3	6052.16	22	vmu	Y?	60	N	Y	N	2,55	H,S	N	
unnamed*	8	148	7,7	6051.71	24	st	N	x	N	N	N	3,18	H,S	N	
unnamed*	35,8	164,4	5,9	6051.13	13	vmu	Y?	80	N	Y	N	1,59	H,S	N	
unnamed*	6,4	83,4	5,1	6052.00	22	vmu	Y?	80	N	Y	Y	2,55	H,S	N	
unnamed*	55	124,5	4,8	6051.51	4	fmJ	Y	x	N	Y	N	2,55	H,S	N	
unnamed*	40,3	105,9	4,4	6051.71	11	vmu	Y	x	N	Y	Y	1,59	H	N	
unnamed	38,7	114,7	4,3	6050.90	11	st	Y	30	N	Y	N	1,59	H	N	Postdates formation of ARF
unnamed*	7,9	74,2	4,2	6051.89	22	vmu	Y	x	N	Y	N	2,55	H,S	N	
unnamed*	52,1	123,2	4	6051.61	4	fmJ	Y	80	N	Y	N	2,23	H,S	N	
unnamed	43	150,9	3,9	6051.05	13	vmu	Y?	40	N	Y	N	2,86	H,S	N	
unnamed*	10,4	136,5	3,8	6051.48	24	vmu	Y	x	N	Y	N	2,23	H,S	N	
unnamed	42,7	141,7	3,8	6051.52	12	vmu	Y?	70	N	Y	N	3,5	H,S	N	
unnamed*	13,2	112,8	3,7	6051.24	23	bst	Y?	x	N	Y	N	1,91	H	N	
unnamed*	13,33	123,46	1,9		24	btu		x	N	Y	N		S	N	
unnamed*	11,9	132,3	3,6	6051.54	24	bst	Y?	x	N	Y	N	2,86	H,S	N	
unnamed*	15,1	116,8	3,6	6051.63	23	bst	Y	80	N	Y	N	3,5	H,S	N	
unnamed*	43,3	67,7	3,6	6050.70	10	vmu	Y	x	N	Y	N	1,91	H,S	N	Postdates formation of ARF
unnamed	22,6	94,1	3,1	6051.43	23	bst	Y	x	N	Y	Y	2,23	H,S	N	
unnamed	29,6	135,4	2,7	6051.14	12	vmu	Y	20	N	Y	N	0,95	H,S	N	
unnamed*	8,5	132,4	4,3	6051.60	24	bst	Y	x	N	Y	N	2,55	H,S	N	
Valentina	46,4	144,1	24,3	6051.39	12	vmu	Y	x	Y	Y	Y	4,14	H,S	N	
Vallija	26,3	120	15	6050.93	11	vmu	Y	200	N	Y	Y	2,86	H,S	N	Postdates formation of ARF and ACWR
Vigee-Lebrun	17,3	141,4	57,6	6051.06	24	vmu, bst	Y?	x	N	Y	Y	2,55	H,S	N	Postdates formation of NW fractures and ACWR
Wharton	55,6	61,9	50	6051.76	3	sf	Y	140	N	Y	Y	1,27	H,S	Y	
Wilder	17,4	122,6	35,3	6052.02	24	rtGe, bst	Y	x	Y	Y	Y	3,18	H,S	N	

Winema	3	168,6	21,1	6051.58	25	fcRu2	Y	x	N	Y	Y	3,18	H,S	N	Postdates N-trending folds
Yakyt	2,1	170,2	13,8	6052.19	25	fcRu2	Y	x	Y	Y	Y?	3,5	H,S	Y	Predates final activity along N-trending fractures
Yazruk	21,2	160,2	10	6051.12	25	fcl	Y	170	N	Y	N	1,27	H,S	N	
Yolanda	7,8	152,7	11,1	6051.76	25	vmu	Y	40	Y	Y	N	1,91	H,S	N	Postdates ARF formation
Ytunde	49,9	81,1	7,7	6051.57	10	sf	Y	x	N	Y	N	1,59	H,S	Y?	
Zivile	48,8	113,1	11	6051.83	11	sf	Y	135	N	Y	N	2,55	H,S	N	Postdates ARF formation
Zulfiya	18,4	101,9	12,3	6051.63	23	bst, st	Y	x	N	Y	N	2,55	H,S	N	Postdates ARF formation, although ARF may also been locally reactivated
Zumrad	32,1	94,8	12,9	6051.16	11	bst	Y	60	N	Y	N	1,91	H,S	N	Postdates ARF formation

Abbreviations: N, no; U, unknown; Y, yes; ACRW, Artemis concentric wrinkle ridges; ARF, Artemis radial fractures.

Dark floor: Materials in the crater floor with the same radar reflectivity than surrounding volcanic materials. Interpreted as possible embayed.

\* Craters not represented in map because of size and map resolution

Venus crater data bases: S, Schaber and others (1992); H, Herrick and others (1997)

Crater density values from Herrick and others (1997) at a crater's location. Value is the density of craters in the neighborhood of the specified crater; that is, the number of craters (including the specified crater) within a 1000 km radius circle normalized to give the number of craters per 1 x 10<sup>6</sup> km<sup>2</sup>.